Available online at www.sciencedirect.com
ScienceDirect
International Journal of Plasticity 24 (2008) 867–895
INTERNATIONAL JOURNAL OF Plasticity
www.elsevier.com/locate/ijplas

A dislocation-based constitutive law for pure Zr including temperature effects

I.J. Beyerlein [a,*], C.N. Tomé [b]

[a] *Theoretical Division, Los Alamos National Laboratory, Los Alamos, NM 87545, USA*
[b] *Materials Science and Technology Division, Los Alamos National Laboratory, Los Alamos, NM 87545, USA*

Received 10 April 2007; received in final revised form 16 July 2007
Available online 17 August 2007

Abstract

In this work, a single crystal constitutive law for multiple slip and twinning modes in single phase hcp materials is developed. For each slip mode, a dislocation population is evolved explicitly as a function of temperature and strain rate through thermally-activated recovery and debris formation and the associated hardening includes stage IV. A stress-based hardening law for twin activation accounts for temperature effects through its interaction with slip dislocations. For model validation against macroscopic measurement, this single crystal law is implemented into a visco-plastic-self-consistent (VPSC) polycrystal model which accounts for texture evolution and contains a subgrain micromechanical model for twin reorientation and morphology. Slip and twinning dislocations interact with the twin boundaries through a directional Hall–Petch mechanism. The model is adjusted to predict the plastic anisotropy of clock-rolled pure Zr for three different deformation paths and at four temperatures ranging from 76 K to 450 K (at a quasi-static rate of 10^{-3} 1/s). The model captures the transition from slip-dominated to twinning-dominated deformation as temperature decreases, and identifies microstructural mechanisms, such as twin nucleation and twin–slip interactions, where future characterization is needed.
Published by Elsevier Ltd.

Keywords: A. Dislocations; A. Twinning; B. Constitutive behavior; B. Crystal plasticity; Hcp zirconium

* Corresponding author. Tel.: +1 505 665 2231; fax: +1 505 665 5926.
E-mail address: Irene@lanl.gov (I.J. Beyerlein).

0749-6419/$ - see front matter Published by Elsevier Ltd.
doi:10.1016/j.ijplas.2007.07.017

1. Introduction

This work is part of a comprehensive study focused on the deformation mechanisms in hcp materials and incorporating them into constitutive laws for the plastic deformation of hcp materials. Our previous work clearly establishes the necessity of applying a crystallographic approach for this pursuit (as opposed to continuum type hardening laws), in order to account for the variety of slip and twinning modes present in the grain, their relative strengths, and their relative activity depending on their orientation with respect to the loading direction. In addition, crystallographic texture and twin evolution strongly influence macroscopic hardening and anisotropy of the mechanical response and therefore, need to be incorporated into constitutive models.

In the past we used Voce-type hardening for the critical resolved shear stress of slip and twinning, and implemented it into a visco-plastic self-consistent (VPSC) polycrystal model (Lebensohn and Tomé, 1993; Tomé and Lebensohn, 2004). Using this approach, constitutive descriptions for Zr applicable to fixed temperatures (76 K or 300 K) (Tomé et al., 2001) and strain path changes (Yapici et al., in press) have been developed. This formulation was later applied to predict the flow response of Zr when the temperature changes from 76 K to 300 K while keeping the test direction fixed (Kaschner et al., 2006). In these applications the treatment of twinning was greatly simplified. Twin reorientation was modeled according to a Predominant Twin Reorientation scheme (Tomé et al., 2001), in which the original grain orientation is replaced by the orientation of its most active twin. Twin–twin or twin–slip interactions were modeled via empirical latent hardening factors, which were assumed to be temperature independent. This twin model proved to be too simplistic for modeling strain path changes, where twins introduced in the pre-load stage act as directional barriers to newly activated systems in the reload stage. As a consequence, we improved the treatment for twinning by representing each twinned grain as a Composite Grain (CG) consisting of layers of twin and matrix (see Fig. 1). This approach allows us to account for the directional barriers that a specific twin poses to specific dislocations via a Hall–Petch effect. With this CG approach, VPSC effectively predicted the texture and hardening evolution when clock-rolled Zr is deformed in compression along the in-plane direction followed by compression along the through-thickness direction (and vice versa) (Proust et al., 2007).

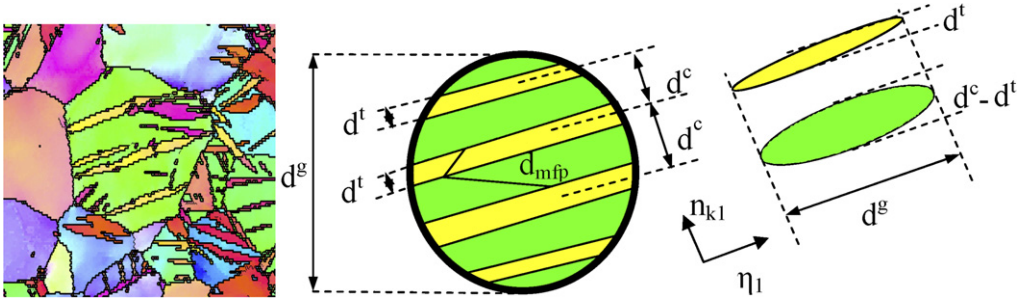

Fig. 1. EBSD image of Zr deformed 5% at 76 K. Schematic of Composite Grain model implemented in VPSC, showing morphology and orientation of twins and matrix, and indicating the parameters of the Composite Grain model.

All the above models contain parameters specific to a given temperature and strain rate, making them difficult to apply to deformation histories involving changes in temperature and strain rate. In this work, we generalize our model to address such limitations, and propose a dislocation-density-based constitutive law for slip in pure hcp metals that accounts for temperature effects. Each slip mode has its own dislocation evolution law that includes thermally-activated recovery processes that lead to either annihilation or debris formation. The corresponding hardening law for slip addresses stages II–IV. The hardening law for twin propagation accounts for temperature effects through its interaction with slip dislocations. The hardening models are implemented into the CG model, where slip and twinning dislocations interact with twin boundaries through a Hall–Petch relationship, and the CG model is, in turn, implemented into the fully anisotropic VPSC polycrystal approach to make the connections between texture evolution, slip and twin activity, single crystal hardening, and macroscopic response.

1.1. Experimental background

Zirconium has been reported to deform by a variety of modes: prismatic $\langle a\rangle$, pyramidal $\langle c+a\rangle$ and basal slip $\langle a\rangle$, two types of tensile twinning: $\{10\bar{1}2\}(10\bar{1}\bar{1})$ and $\{11\bar{2}1\}(11\bar{2}\bar{6})$, and two types of compression twinning: $\{11\bar{2}2\}(11\bar{2}\bar{3})$ and $\{10\bar{1}1\}(10\bar{1}\bar{2})$ (Rapperport and Hartley, 1960; McCabe et al., 2007; Kaschner et al., 2006; Yoo, 1969; Yoo and Wei, 1966; Reed-Hill et al., 1965; Akhtar, 1973b, 1975; Akhtar and Teghtsoonian, 1971). The active modes and their relative contribution to deformation depend on strain level, temperature, strain rate, direction of loading, and purity level. Deformation is further complicated by the fact that each mode has its own sensitivity to temperature and strain rate. Understanding the deformation behavior of Zr (texture evolution, plastic anisotropy, hardening rate) requires not only knowing which of these mechanisms operate, but also how they interact.

Some of the most comprehensive work on Zr single crystals was performed by Akhtar and co-workers (Akhtar, 1973b, 1975; Akhtar and Teghtsoonian, 1971). Akhtar and Teghtsoonian (1971) studied the tensile behavior of single crystal Zr over a wide range of temperatures and orientations. Prismatic slip was found to be the easiest slip mode in all conditions, followed by $\{10\bar{1}2\}$ tensile twinning up to 850 K. Above 850 K, both prismatic and basal slip were observed but no twinning. In c-axis compression (Akhtar, 1973b), Zr crystals deformed by $\{11\bar{2}2\}$ compressive twinning (CTW) below 800 K, and by pyramidal $\langle a\rangle$ slip plus $\{10\bar{1}1\}$-twinning above 800 K. Pyramidal slip $\langle a\rangle$ was found to be extremely temperature sensitive and with a critical resolved shear stress 10–20 times higher than that for prismatic or basal at the same temperature.

Previous work done on polycrystalline Zr suggests that it is possible for deformation modes not observed in single crystal experiments to be active inside aggregates. The reason is likely to be stress concentrations and multislip induced by grain boundary constraints. In our previous studies of clock-rolled pure Zr (Tomé et al., 2001; Kaschner et al., 2006; Proust et al., 2007), the texture allowed us to selectively activate certain deformation modes, much like in a single crystal. Our observations are similar to those reported in Reed-Hill et al. (1965). Compression along the in-plane direction of the plate puts the basal component of the texture under tension and, as in the single crystal tests, prismatic slip and $\{10\bar{1}2\}$ tensile twinning are observed. The contribution of tensile twinning was higher at 76 K than at 300 K. Tension along the in-plane direction is overwhelmingly

accommodated by prismatic slip. Compression along the plate normal is accommodated by $\{11\bar{2}2\}$ compressive twinning at 76 K, but by pyramidal $\langle c+a\rangle$ slip at room temperature. TEM and EBSD analyses confirm the presence or absence of these mechanisms (McCabe et al., 2007).

1.2. Theoretical background

Models for polycrystalline flow response in hcp materials have been derived from crystal plasticity (Plunkett et al., 2006; Cazacu et al., 2006; Sarma and Zacharia, 1999), micromechanical phenomenological laws (Dunlop et al., 2006; Chen and Gray, 1997; Reed-Hill et al., 1963), or from polycrystal homogenization schemes which assign a critical resolved shear stress for each slip and twin mode (Plunkett et al., 2006; Salem et al., 2005; Walde and Riedel, 2003; Tomé et al., 2001; Kaschner et al., 2006; Yapici et al., in press; Yu et al., 2005).

For modeling temperature (and strain rate) effects in hcp metals, a model based on rate-controlled mechanisms is necessary, and thermally-activated flow is usually assumed. Single crystal models of this sort focus only on basal or prismatic slip (Friedel, 1963; Seeger et al., 1963; Dorn and Mitchell, 1964), with the exception of Lavrentev (1980) who considered different slip populations. Other thermal-activation models treat the hcp aggregate as an effective continuum (Dunlop et al., 2006; Reed-Hill et al., 1995; Chen and Gray, 1997). Although these models compared well to the measured yield stresses of single crystal Bi (hex), Zn, and Cd (Kuhlmann, 1951), and polycrystalline Ti and Zr alloys, they do not address plastic anisotropy, texture, relative activities of different slip and twinning modes, and twin reorientation.

The dislocation-based thermally-activated hardening model developed here is used to predict the flow response of textured pure Zr (<100 ppm) reported in (Beyerlein et al., 2007). There, Zr was tested in tension and compression along different directions, over a wide range of temperatures (76–450 K), and at a quasi-static rate of 10^{-3} 1/s. For this application, the model considers the four deformation modes observed previously via microscopy analyses in this Zr (McCabe et al., 2007): prismatic slip, pyramidal $\langle c+a\rangle$ slip, tensile twinning $\{10\bar{1}2\}(10\bar{1}\bar{1})$, and compressive twinning $\{11\bar{2}2\}(11\bar{2}\bar{3})$. Parameters coupling slip and twinning and for strain rate effects are introduced in the formulation but not explored fully here. In a future paper, slip–twin interactions will be investigated more deeply through a series of temperature and strain path change tests and using the multi-scale model developed here.

2. Polycrystal and twin orientation modeling

To model the macroscopic response of a textured aggregate we use the polycrystal visco-plastic self-consistent (VPSC) formalism (Tomé and Lebensohn, 2004; Lebensohn and Tomé, 1993). Individual grain deformation takes place by slip and twinning, and depends on grain orientation, grain shape, and grain interaction with the surrounding homogeneous medium. The latter possesses anisotropic properties calculated self-consistently as the average behavior of all the grains. These features are not only advantageous but necessary for modeling low-symmetry polycrystals, such as Zr, which deform anisotropically. Texture and hardening evolution, which are updated incrementally during the simulation, are crucial for judging the soundness of the model. Comparisons against

mechanical test data and TEM and EBSD evidence allow us to infer indirectly the characteristics of the slip–slip, twin–twin and twin–slip interactions.

To model twinning reorientation, twin evolution, and twin barriers, we utilize the uncoupled version of the CG twin model recently proposed by (Tomé and Kaschner, 2005; Proust et al., 2007). In this model, when the volume fraction in the Predominant Twin System in a given grain reaches a critical value the grain is split into matrix and twin regions (Fig. 1). The twin domain is given a flat ellipsoidal shape (short axis perpendicular to the twin plane) with twin orientation, while the matrix is also split into ellipsoidal domains parallel to the twin. As deformation proceeds the twin and matrix ellipsoids, are allowed to grow and shrink, respectively, but each of them interacts only with the effective medium and not directly with each other. This assumption can be justified on the basis of our observations that twins in Zr can grow to be as large as grains. Twin nucleation is not explicitly treated here and enters indirectly in the formulation through an empirical delay in twinning activation (see Section 3.4).

In the CG model the contribution to shear $\Delta\gamma^s$ of each twin system s in each grain is followed. When the volume fraction in a system $f^s = \Delta\gamma/S$ reaches a threshold (5%), this system is selected as the PTS in the grain (where S is the characteristic twin shear). In all grains, the twinned regions are equally spaced and have equal thickness (see Fig. 1). The parameter d_c defines the center-to-center spacing between neighboring twins, and f_{max} is the maximum allowable volume fraction of twinning in any given grain. d_t is the evolving twin width. d_c and f_{max} are set based on microscopy data and are not adjusted freely to fit data. As in the previous work (Proust et al., 2007), d_c is 0.2 d_g for tensile twinning and 0.05 d_g for compressive twinning and f_{max} is 50%. d_g is the grain size.

A key element in the CG model is the mean free path d_{mfp} which is defined by the combined crystallography of the predominant twin system (PTS) and that of the other slip s or twin systems t. This directional mean free path enters in the hardening law and evolves with twin activity from a maximum $d_{mfp} = d_g$ (when no twin is present) to a minimum of d_t within the twin, or $(d_c - d_t)$ within the matrix (see Fig. 1).

3. Single crystal hardening laws

3.1. Flow rule for slip and twinning

Let α represent the slip mode (i.e., prism or pyramidal) and $s \in \alpha$ mean that slip system s belongs to slip mode α. The shear increment $d\gamma^\alpha$ for each slip mode α is a straightforward sum of the shears of all slip systems contained in mode α:

$$d\gamma^\alpha = \sum_{s\in\alpha} |\dot{\gamma}^s| \mathrm{d}t \tag{3.1}$$

where

$$\dot{\gamma}^s = \dot{\gamma}_0 \left| \frac{m^s : \sigma}{\tau_c^s(\dot{\varepsilon}, T)} \right|^n \mathrm{sign}(m^s : \sigma) \tag{3.2}$$

This flow rule introduces a critical strength or slip resistance τ_c^s that depends on the local microstructure encountered by the dislocations. Eqs. (3.1) and (3.2) are also used to describe the kinematics of twinning: β denotes the twin type, $t \in \beta$ means that the twin system t is contained in mode β, and τ_c^t is the (directional) threshold required to propagate

this twin system. The exponent n is set high, $n = 20$, so that slip or twinning is activated only when the resolved shear stress closely approaches the critical strength. In Eq. (3.2), $\dot{\gamma}_0$ is set equal to the macroscopic strain rate modulus in order to avoid introducing a rate dependence via n.

Table 1 provides the slip and twin modes considered in this work and the number of systems contained in each. Note that we do not consider basal slip, first-order pyramidal slip, or the much less relevant $\{1\,1\,\bar{2}\,1\}$ tensile twins and $\{1\,0\,\bar{1}\,1\}$ compressive twins. These choices are motivated by previous TEM and OIM analyses of this material (McCabe et al., 2007) and by previous success in modeling texture evolution and plastic anisotropy using VPSC and Voce hardening laws (Tomé et al., 2001; Kaschner et al., 2006). Further discussion on alternative slip and twinning modes is found at the end of the paper.

3.2. Evolution of dislocation density

3.2.1. Thermally-activated glide

In thermally-activated glide, mobile dislocations in pure metals get pinned many times and at many points along their length due to interactions with other dislocations. The rate of plastic strain is controlled by the rate at which thermal energy can help these segments overcome their energy barriers, allowing the rest of the dislocation to bow out, spread, until stopped again.

Dislocation interactions have been classified as either attractive or repulsive (Hirsch, 1959; Whelan, 1959; Friedel, 1963; Seeger et al., 1963; Saada, 1963). The attractive interactions involve pairs of dislocations that either annihilate or recombine, such as in junction or jog formation. While these reactions lower the energy, the mechanisms that enable them, such as cross-slip, or the formation of reaction products, such as constrictions, jogs, and sessile components, cost energy. Repulsive interactions, on the other hand, require less work to overcome, and do not usually transform the dislocations or leave residual components after the interaction. Dislocations easily pull away after having been forced to pass the repulsive obstacle by an external stress. Accordingly, attractive interactions require thermal activation and are said to be temperature-dependent, while repulsive ones are not (Saada, 1963; Friedel, 1959).

Thermal energy is supplied by random thermal fluctuations, and dislocation motion depends on the number of fluctuations that supply the interacting segments the energy they need. The number of such successful outcomes is $n_s = nP(\text{success})$, where n is the number of attempts in the crystal. The probability of success is the probability that the thermal jump U is greater than G, the energy required to surmount the barrier and assumed to follow an Arrhenius law (Eyring, 1936; Becker, 1925; Burgers, 1940), i.e.,

$$P(\text{success}) = P(U > G) = \exp(-G/kT). \tag{3.3}$$

Table 1
Slip and twinning modes used in this work for Zr

Symbol	Mode	Crystallography	S	No. of system	b (nm)
$\alpha = 1$	Prismatic $\langle a \rangle$	$\{1\bar{1}00\}\langle 11\bar{2}0\rangle$	–	3	3.231E-01
$\alpha = 2$	Pyramidal $\langle c + a \rangle$	$\{10\bar{1}1\}\langle 11\bar{2}3\rangle$	–	12	6.077E-01
$\beta = 1$	Tensile twinning	$\{10\bar{1}2\}\langle 10\bar{1}\bar{1}\rangle$	0.167	6	6.326E-01
$\beta = 2$	Compressive twinning	$\{11\bar{2}2\}\langle 11\bar{2}\bar{3}\rangle$	0.225	6	9.236E-02

Considering the strain gained at each successful attempt leads to the thermal-activation controlled expression for the plastic strain rate $\dot{\varepsilon}_p$ which is

$$\dot{\varepsilon}_p = \dot{\varepsilon}_0 \exp(-G(\tau_s)/kT) \tag{3.4}$$

where the prefactor $\dot{\varepsilon}_0$ is a material value (Burgers, 1940; Kocks et al., 1975), that has units of strain rate and depends on the average waiting time at the intersection point, the strain released after the events, and the frequency of thermal fluctuations, which is some fraction of the Debye frequency ($\sim 10^{13}$ s^{-1}). For Cu, Ag (Follansbee and Kocks, 1988; Kok et al., 2002), Zr (Chen and Gray, 1997), and Mg (Dorn and Mitchell, 1964), $\dot{\varepsilon}_0 \sim 10^7\ s^{-1}$. *$\dot{\varepsilon}_p$ and $\dot{\varepsilon}_0$ are not expected to vary appreciably in time or with straining.*

In Eqs. (3.3) and (3.4) note that $G(\tau_s)$ is a function of τ_s, which is a concentrated shear stress due to the short-range interaction with another dislocation (or obstacle), emphasizing the localized nature of thermally-activated events. It is also common to attribute G or Eq. (3.4) to one type of thermally-activated process. This simplification applies when one process has a much smaller G than the rest. Thermally controlled plastic deformation, however, is a complex collective phenomenon of many thermally-activated processes. To continue to use this theory, G must be treated as an effective energy covering all possible types of such processes.

There are several possible outcomes of successful thermally-activated reactions, depending on the type of interaction (Seeger et al., 1963; Saada, 1963; Friedel, 1963; Essmann and Mughrabi, 1979; Hirth and Lothe, 1982; Gilman, 1969). (i) Production of jogs by interactions between gliding dislocations with an attractive forest, (ii) production of dipoles by jog motion, (iii) production of defects by cross-slip, (iv) junction formation (e.g. Lomer-Cottrell locks), and (v) annihilation of oppositely-signed dislocations or absorption into grain boundaries.

As a result of (i–v), there is a dislocation population, ρ_{rem}, that is removed from the population ρ either as defects ρ_{deb} (i–iv) or by recovery ρ_{ann} (iv, v). The rate of accumulation of ρ under straining is the difference between the rate of generation (or storage) and the rate of removal:

$$\begin{aligned}\frac{\partial\rho}{\partial\gamma} &= \frac{\partial\rho_{\text{generation}}}{\partial\gamma} - \frac{\partial\rho_{\text{rem}}}{\partial\gamma} = \frac{\partial\rho_{\text{generation}}}{\partial\gamma} - f\frac{\partial\rho_{\text{rem}}}{\partial\gamma} - (1-f)\frac{\partial\rho_{\text{rem}}}{\partial\gamma} \\ &= \frac{\partial\rho_{\text{generation}}}{\partial\gamma} - \frac{\partial\rho_{\text{deb}}}{\partial\gamma} - \frac{\partial\rho_{\text{ann}}}{\partial\gamma}\end{aligned} \tag{3.5}$$

where f is the fraction of ρ_{rem} that is transformed into debris and $(1-f)$ that is annihilated.

3.2.2. Evolution model for dislocation density

Most dislocation density-based models for thermally-controlled evolution have been developed for fcc materials for a single slip mode, and up to stage III only. There, the prevalence of the thermal activation regime has been loosely applied to strain rates covering $\dot{\varepsilon} \sim 10^{-5}$–$10^3$ 1/s. One of the most widely used thermal activation models is the one by Essmann and Mughrabi (1979) and further developed by Mecking and Kocks (1981, 2003):

$$\frac{\partial\rho^\alpha}{\partial\gamma^\alpha} = k_1^\alpha\sqrt{\rho^\alpha} - k_2^\alpha(\dot{\varepsilon}, T)\rho^\alpha \tag{3.6}$$

In the remainder of Section 3, Eq. (3.6) is extended for hcp materials and the debris population in Eq. (3.5) is formulated and linked to stage IV hardening. Note that to appreciate the various slip modes that can operate in these materials, we have added the superscript α to refer to a particular slip mode, so that Eq. (3.6) becomes the evolution law for a particular dislocation population α.

3.2.3. Dislocation generation

Many mechanisms have been proposed for dislocation generation, either sources from which dislocation loops are emitted, e.g. Frank-Read sources (Essmann and Mughrabi, 1979), or those that aid propagation of mobile dislocations and nucleation of more sources, e.g. cross-slip (Friedel, 1959; Gilman, 1969). Generally they involve expansion from pre-existing line lengths pinned at one or two points. Hence, the rate of generation is determined by the initial density, current density ρ, distances λ for free expansion, and the rate at which sources can produce loops. Due to the nature of dislocation motion in thermally-activated glide, the rate of dislocation production is directly proportional to the rate of dislocation storage, which increases inversely with λ, variously defined by solute spacing, impenetrable obstacle spacing, subboundary spacing, grain size, or in Eq. (3.6), dislocation spacing $\rho^{-1/2}$ (Essmann and Mughrabi, 1979; Mecking and Kocks, 1981; Estrin and Mecking, 1984; Follansbee and Kocks, 1988; Kok et al., 2002). Also in thermally-activated glide, processes involving dislocation multiplication are rate insensitive compared to the dislocation removal processes discussed above. For the $10^{-3}\ s^{-1}$ condition studied here, it is reasonable make the coefficient k_1 in the model equation (3.6) solely a function of material, and not of strain rate or temperature. However for strain rates beyond $10^3\ s^{-1}$, the initial hardening rate of a variety of metals begins to increase significantly with strain rate (e.g. Follansbee and Kocks, 1988; Klepaczko, 1991) and the rate of dislocation production would not be independent of strain rate.

3.2.4. Dislocation removal

Writing Eq. (3.4) for each slip mode α with the appropriate superscript on G^α and τ_s^α, setting $\dot{\varepsilon}_p^\alpha$ equal to the applied strain rate $\dot{\varepsilon}$ for each crystal, and assuming $\dot{\varepsilon}_0$ is the same for all slip modes, fix τ_s^α to be

$$\tau_s^\alpha = H^\alpha(kT\ln(\dot{\varepsilon}_0/\dot{\varepsilon})) \tag{3.7}$$

where H^α is the inverse function of $G^\alpha(\tau_s^\alpha)$. Eq. (3.7) implies that the local resolved shear stress does not vary appreciably from a value fixed by $\dot{\varepsilon}$ and T. This is one of the key criteria for using thermal activation theory for plasticity: *local internal stresses cannot become too high* (Gilman, 2002).

According to Eq. (3.6), as the crystal is strained, the rate of removal will eventually catch up with the rate of generation such that a steady-state value of ρ^α is reached, denoted as $\rho_{sat}^\alpha = (k_1^\alpha/k_2^\alpha)^2$. k_2^α is defined so that τ_s^α in Eq. (3.7) equals τ_{sat}^α, the shear stress associated with ρ_{sat}^α. Letting l_{sat} be the average spacing between dislocations in population ρ_{sat}^α, then $\tau_s^\alpha = \tau_{sat}^\alpha = \chi\mu b/l_{sat} \sim \chi\mu b\sqrt{\rho_{sat}^\alpha}$, and:

$$\frac{k_2^\alpha(\dot{\varepsilon},T)}{k_1^\alpha} = \frac{\chi b^\alpha \mu}{\tau_{sat}^\alpha(\dot{\varepsilon},T)} \tag{3.8}$$

where χ is an interaction parameter between 0.1 and 1.0 (see Section 3.3.4) and μ is the shear modulus.

At this stage an expression for $G(\tau_s)$ is desired, where τ_s is the short-range stress at the intersection point. In one of the original thermal activation models, applied at the time to liquids (Eyring, 1936), $G = G_0 - af$, where f is the force applied *at the molecule*, a, a volume, and G_0 the energy barrier with $f = 0$. A similar result is produced from a first-order Taylor's series expansion of $G(\tau)$ about zero (Saada, 1994; Friedel, 1963)

$$G^\alpha(\tau_s) = G^\alpha(0) + \frac{\partial G^\alpha}{\partial \tau_s^\alpha}(\tau_s) \approx G_0^\alpha - \mathrm{vol}_{\mathrm{act}}^\alpha \tau_{\mathrm{sat}}^\alpha \tag{3.9}$$

where $vol_{act} = -\partial G/\partial \tau_s$ is interpreted as an activation volume, $G_0^\alpha = G^\alpha(0)$, and τ_s^α is set to $\tau_{\mathrm{sat}}^\alpha$. In Eq. (3.9), G_0^α and vol_{act} are not necessarily independent of the current stress-state in the material. Generally as τ_s increases, $G(\tau_s)$ decreases, a tendency observed in Zr single crystals (Mills and Craig, 1968). Consider that G_0^α and vol_{act} are both inversely proportional to τ_{sat} in a similar manner,

$$G_0^\alpha = \frac{D^\alpha}{\tau_{\mathrm{sat}}^\alpha}[g^\alpha \mu b^3] \tag{3.10a}$$

$$\mathrm{vol}_{\mathrm{act}}^\alpha = \frac{D^\alpha}{\tau_{\mathrm{sat}}^\alpha}[b^3] \tag{3.10b}$$

where g^α is a normalized, stress-independent activation energy (Kocks et al., 1975), D^α is a proportionality factor with units of stress, and $D^\alpha > \tau_{\mathrm{sat}}^\alpha$. The quantities in brackets are what is typically used for G_0^α and $\mathrm{vol}_{\mathrm{act}}$. Making these substitutions in Eq. (3.9), the rate equation changes to

$$\dot{\varepsilon} = \dot{\varepsilon}_0 \exp\left(-\frac{D^\alpha b^3 (g^\alpha \mu - \tau_{\mathrm{sat}}^\alpha)}{kT} \cdot \frac{1}{\tau_{\mathrm{sat}}^\alpha}\right) \tag{3.11}$$

Finally, inserting Eq. (3.11) into Eq. (3.8), we have for k_2^α,

$$\frac{k_2^\alpha(\dot{\varepsilon}, T)}{k_1^\alpha} = \frac{\chi b^\alpha}{g^\alpha}\left(1 - \frac{kT}{D^\alpha b^3} \ln\left(\frac{\dot{\varepsilon}}{\dot{\varepsilon}_0}\right)\right) \tag{3.12}$$

We set $\dot{\varepsilon}_0$ to $10^7\ \mathrm{s}^{-1}$ for both slip modes and with this, Eq. (3.12) predicts that k_2^α increases with T for the range of $\dot{\varepsilon}$ where this equation is applicable (10^{-5}–$10^3\ \mathrm{s}^{-1}$).

Some gross assumptions were made in order to derive Eq. (3.12) and to describe some very complex phenomena. Surprisingly, however, Eq. (3.12) will turn out to be effective. Measurements in several materials consistently suggest that under very low stresses dislocation velocities v best follow an exponential law, $v \sim \exp(-D/\tau)$, where D is interpreted as a drag stress (Gilman, 2002; Mordehai et al., 2003). Also Gilman (2002) showed that accounting for the 2-D dislocation motion in their pathway to overcome barriers leads to a similar dependence. Comparison with the Arrhenius expression for dislocation velocity in Eq. (3.11) implies that D decreases with T, as is the case for fcc materials, e.g. see Mordehai et al. (2003). As we will show later, in spite of the linearization applied in Eq. (3.9), the resulting Eq. (3.12) provides a non-linear stress–temperature relationship that is more sensitive at high temperatures than at low temperatures, that is observed in pure Zr. Higher order terms are therefore not needed in Eq. (3.9) and would only add more parameters.

Many of the model expressions above, like Eqs. (3.8) and (3.10) include the shear modulus μ. While Zr is elastically anisotropic, data in (Fisher and Renken, 1964) suggest that

the temperature dependence of μ is much greater than its dependence on shearing direction. Thus, it is reasonable to use an 'effective' μ, which is an average value of the three main shear moduli, c_{44}, c_{55}, and c_{66} at a given temperature. The reduction in this effective μ with temperature can be represented well with the following linear relationship with T:

$$\mu = 40.06\ \text{GPa} - 0.022T\ \text{GPa}/K \tag{3.13}$$

For hcp materials which are elastically very anisotropic, one may want to use the value of μ associated with the slip plane and direction of the slip mode.

3.2.5. Debris generation

The creation of debris involves a strong coupling between various slip modes and cannot generally be associated with one mode α. Debris can be formed by reactions between any two types of slip dislocations, and can consist of segments left behind on any one of the many slip planes found in Zr. The total population ρ_{deb} will be composed of all types of dislocations, $\langle a\rangle$ and $\langle c+a\rangle$, and $\langle c\rangle$ as well. (Although $\langle c\rangle$ dislocations are not directly accounted for here, they could be thought of as debris, such as when pyramidal $\langle c+a\rangle$ cross slips onto the basal plane.) Accordingly, consider the evolution of ρ_{deb} as a function of the sum of debris contributed by each mode, $f^{\alpha}\partial\rho^{\alpha}_{\text{rem}}$,

$$\partial\rho_{\text{deb,tot}} = q\sum_{\alpha} f^{\alpha}\frac{\partial\rho^{\alpha}_{\text{rem}}}{\partial\gamma^{\alpha}}\,\mathrm{d}\gamma^{\alpha} \tag{3.14}$$

where q is the rate coefficient which reflects how debris can grow from point defects seeded by the local thermal-activated reactions. The numerous possible interactions and intersections for debris formation prevent developing a micromechanically-based expression for f^{α}. We can however reasonably assume that first, f^{α} has some relationship with the current amount of debris in the crystal, and second, debris segments are smaller than the debris spacing. With this, we fix the ratio of line length of debris, some multiple n of b, to the average spacing between debris, and assign f^{α} to this ratio:

$$f^{\alpha} = \frac{nb^{\alpha}}{l_{\text{deb}}} \approx A^{\alpha}b^{\alpha}\sqrt{\rho_{\text{deb}}} \tag{3.15}$$

Together with Eq. (3.14), this expression for f^{α} implies that debris storage rates increase with the amount of debris collected in the material, which is to be expected. Microstructural observation suggests that, when passing through or reacting with existing debris or substructure, gliding dislocations leave behind more debris (Dai and Victoria, 1997). For prismatic dislocations, we find that f^{1} increases slightly with temperature at low temperatures, possibly related to an increase in the interaction length between dislocations as temperature increases (Essmann and Mughrabi, 1979). Specifically A^{1} is made to vary with T as $A^{1} = 37\ \ln(1 + T/30\ \text{K})$. For pyramidal dislocations, f^{2} is insensitive to T.

In Eq. (3.14), interaction terms, such as $\partial\rho^{\alpha}_{\text{rem}}\partial\rho^{\alpha\prime}_{\text{rem}}$, or the production of a defect population of $\langle c\rangle$-dislocations is neglected. Also mechanisms for debris reduction are also neglected for the temperature interval studied here, which means that ρ_{deb} will not saturate. With the aid of thermal energy, mechanical work (by internal stress), or interactions from sweeping dislocations, sessile debris segments can in time collapse, reduce in length, or relax into stable configurations. Tangled dislocation structures can then transform into well-defined networks, lowering the overall internal energy. While these improvements in

the debris formulation could be included, it was not necessary for the temperature and strain range studied here.

3.3. Resistance to slip

3.3.1. Impact on work hardening of the polycrystal

Thermally-activated processes are enhanced by increases in T and decreases in $\dot{\varepsilon}$, and generally become prevalent after some amount of straining. The onset of significant thermally-activated events is observed to reduce the macroscopic work hardening rate. As the saturation point occurs in an increasing number of grains, the hardening rate of the polycrystal is said to transition from stage II to stage III. Consistent with the theories of Essmann and Mughrabi (1979) and Mecking and Kocks (1981), the onset of stage III in many materials is found to be rate sensitive. Microscopically the rate-sensitivity of removal is controlled by k_2 Eq. (3.6) for each slip mode in each crystal, which increases with T and decreases with $\dot{\varepsilon}$.

In Zr, as in most polycrystalline metals, non-zero work hardening can continue beyond stage III at large strains (typically >30% strain) and usually at a constant rate. Compared to stages I – III, the mechanisms behind this subsequent linear work hardening stage, stage IV, are less well understood (see Kocks and Mecking, 2003). In modeling, stage IV hardening has been related to the morphology or dimensions of the substructure within grains in the later stages of straining, e.g. cell sizes, spacing between geometrically necessary dislocations, lamellar spacing (Kok et al., 2002; Estrin et al., 1998; Haasen, 1989; Argon and Haasen, 1993). To date, however, the relationships between particular microstructural features and the rate of stage IV hardening still remain unclear. Furthermore the formation of well-defined substructure in Zr has not been well-characterized to date, yet stage IV deformation is quite clear in our Zr results (Beyerlein et al., 2007). Alternatively stage IV has been linked to debris generation (Kocks and Rollett, 1994; Rollett et al., 1987). Debris can act as obstacles to gliding dislocations and result in work hardening, even after ρ_{sat} is reached. Kocks and Rollett (1994) proposed that the accumulation of dislocation debris is a fraction of the rate of dynamic recovery, as described in Section 3.2.1. A link between the rate of debris and the rate of recovery implies a direct relationship between stage III hardening, via ρ_{sat}, and stage IV hardening, ρ_{deb}. In agreement, observations of fcc materials have suggested that the stage IV hardening rate is roughly proportional to τ_{sat}, $\theta_{\text{IV}} = c\tau_{\text{sat}}$, where $c = 0.05$–0.1 (Rollett et al., 1987; Langford and Cohen, 1969).

3.3.2. Contributions to slip resistance

Work hardening is linked to the evolution of dislocations, their mutual interactions, and their interactions with barriers in the microstructure. In the model, τ_{c}^{α} includes contributions from forest dislocations, debris, and twin boundaries:

$$\tau_{\text{c}}^{\text{s}} = \tau_0^{\alpha} + \tau_{\text{forest}}^{\alpha} + \tau_{\text{deb}}^{\alpha} + \tau_{\text{HP}}^{\text{s}} \quad s \in \alpha \tag{3.16}$$

τ_0^{α} is the initial slip resistance which depends on slip mode α, solute density, and T and $\dot{\varepsilon}$ due to interactions with alloying elements. The second and third terms represent the work hardening due to dislocation interactions. The last term $\tau_{\text{HP}}^{\text{s}}$ is the barrier effect provided by grain or twin boundaries, whichever constrains the mean free path more.

3.3.3. Initial slip resistance

For Zr, we consider τ_0^α separately for prismatic, $\alpha = 1$, and pyramidal $\langle c + a \rangle$ slip, $\alpha = 2$. Measurements for τ_0^α in Zr single crystals of lower purity can be found for prismatic slip in (Mills and Craig, 1968; Soo and Higgins, 1968), and for pyramidal $\langle c + a \rangle$ and basal above 800 K in (Akhtar, 1973a,b, 1975). Without any comparable data for our Zr we estimate τ_0^α by comparing polycrystal calculations for initial yield with measurements at different temperatures. CRSS values for prism slip in Mg (Flynn et al., 1961) and pyramidal slip in Be (Garber et al., 1963) have been shown to decay exponentially with T. Fitting this relation to our model estimates for τ_0^α at 76 K, 150 K, 293 K and 450 K, we obtain:

$$\tau_0^1 = 40.8 \exp\left(-\frac{T}{305\ \mathrm{K}}\right) \tag{3.17}$$

for prismatic $\langle a \rangle$ and

$$\tau_0^2 = 722.5 \exp\left(-\frac{T}{200\ \mathrm{K}}\right) \tag{3.18}$$

for pyramidal $\langle c + a \rangle$. Fig. 2 compares Eqs. (3.17) and (3.18) with our estimates for the four discrete temperatures. In (Mills and Craig, 1968), for Zr single crystals oriented primarily for prismatic glide, the initial yield stress and temperature sensitivity was observed to decrease with temperature and purity level. The results for their purest Zr (130 ± 33 ppm by weight) are also shown in Fig. 2 and agree well with our estimates for prism slip. The temperature dependence of τ_0^1 in Zr has been attributed to either overcoming oxygen atoms (Mills and Craig, 1968; Soo and Higgins, 1968), or to a reduction in stacking fault energy of prismatic dislocations with increased oxygen content (Akhtar, 1975), or to the rate sensitivity of prismatic screw mobility (Monnet et al., 2004).

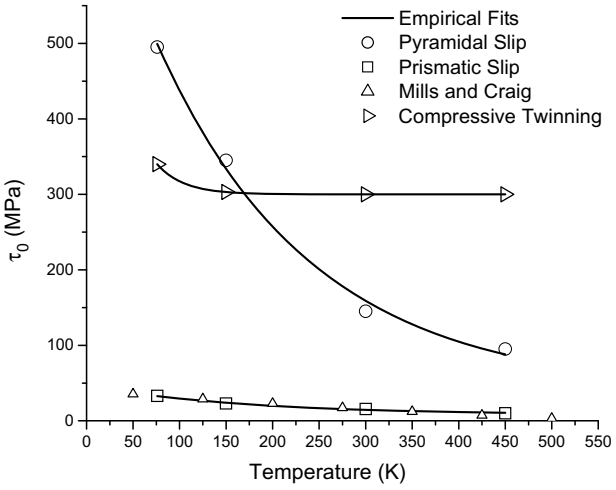

Fig. 2. Variation of initial slip resistance τ_0 with temperature for prismatic $\langle a \rangle$ ($\alpha = 1$), pyramidal $\langle c + a \rangle$ slip ($\alpha = 2$), and $\{11\bar{2}2\}$ compressive twinning for pure Zr (<100 ppm). For $\{10\bar{1}2\}$ tensile twinning $\tau_0 = 20$ MPa independent of temperature. Data from Mills and Craig (1968) for prismatic slip are shown for their purest Zr tested (130 ppm).

Observations from the relatively fewer studies on pyramidal $\langle c+a\rangle$ slip (Garber et al., 1963; Tonda and Ando, 2002; Akhtar, 1976; Blish and Freeland, 1969; Price, 1963; Stohr and Poirier, 1972) demonstrate that the temperature dependence of τ_0^2 for pyramidal $\langle c+a\rangle$ is even more complicated and extreme than it is for prismatic. In (Tonda and Ando, 2002), from 76 K to 150 K, the yield stress of Cd decreases rapidly (by nearly 90%) when oriented for pyramidal slip. Similarly the yield stress of Be in c-axis compression, where the primary system is known to be pyramidal slip, also reduces dramatically, from 76 K to room temperature, by 50–75% (Garber et al., 1963). Fig. 2 shows that, as in single crystal Cd, Co, Zn, Mg, and Be (Garber et al., 1963; Tonda and Ando, 2002; Akhtar, 1976; Blish and Freeland, 1969; Price, 1963; Stohr and Poirier, 1972), τ_0^2 for our Zr also decreases rapidly with increasing temperature, from 500 MPa at 76 K to 95 MPa at 450 K The strong temperature dependence of pyramidal $\langle c+a\rangle$ slip as compared to prismatic slip could be attributed to differences in the way these two dislocations move (Hirth and Lothe, 1982). Prismatic dislocations move as dissociated partials with a fault width, whereas pyramidal $\langle c+a\rangle$ dislocations glide as zonal dislocations, involving shuffling motions that could be aided by thermal energy. As with low temperatures, we can also expect a strong rate-dependence in τ_0^2 for pyramidal slip with high strain rates.

3.3.4. Forest term

It has been shown experimentally on a variety of metals of all crystal structures that the effective slip resistance (minus an initial athermal stress) scales as the square root of dislocation density (Mecking and Kocks, 1981; Lavrentev, 1980). One can derive this relationship by considering the slip resistance provided by forest dislocations spaced l apart to be $\sim\mu b/l$, where for a random arrangement, $l\sim 1/\sqrt{\rho}$. We apply it to describe the resistance encountered by gliding α-dislocations by a forest of α-dislocations:

$$\tau^{\alpha}_{\text{forest}} = b^{\alpha}\chi\mu\sqrt{\rho^{\alpha}} \tag{3.19}$$

where the dislocation interaction coefficient usually ranges in $0.1<\chi<1.0$ (Lavrentev, 1980), but has been reported to be as high as 2. While considered independent of strain, χ contains a "trivial strain-rate and temperature dependence" (Mecking and Kocks, 1981) when derived from thermal activation considerations (Mecking and Kocks, 1981; Lavrentev, 1980) by

$$\chi = \hat{\chi}s(\dot{\varepsilon},T)$$

where $\hat{\chi}$ is close to unity and $s(\dot{\varepsilon},T)$ increases from 0 to 1 as T decreases to zero. For the range of T tested here, and $\dot{\varepsilon}=10^{-3}$ 1/s, and using suitable parameters for prismatic slip in Zr, we find that $s(\dot{\varepsilon},T)$ ranges between 3/4 and 1. Rather than introducing extra parameters associated with $s(\dot{\varepsilon},T)$ for each slip mode, we assign $\chi=0.9$ and do not vary it to fit the data.

Note that Eq. (3.19) is a simplification because it only considers forest interactions between the same type of dislocation. However in Zr the forest can consist of a mix of dislocation-types. Extensions of this model to incorporate such coupling will be discussed later.

3.3.5. Debris contribution (stage IV)

Most of the debris leading to stage IV hardening is thought to be locked in groups or relaxed into stable structures. Generally the barrier provided by a stable grouping of

dislocations with a given spacing depends on the morphology and size of the group. For instance, for a linear array with spacing d, the dislocation needs to overcome a force $\sim d^{-1}$. Unlike forest dislocations, the arrangement of debris, perhaps as part of sub-boundaries, will not be random and a relationship such as Eq. (3.19) cannot be used. For the contribution by ρ_{deb}, we apply a slightly different form, as found in dislocation dynamics studies by (Madec et al., 2002)

$$\tau^{\alpha}_{\text{deb}} = k_{\text{deb}}\mu b^{\alpha}\sqrt{\rho_{\text{deb}}}\log\left(\frac{1}{b^{\alpha}\sqrt{\rho_{\text{deb}}}}\right) \tag{3.20}$$

The above is related to the stress required for gliding dislocations to bow out and punch through arrays of locked dislocation segments spaced by $1/\sqrt{\rho_{\text{deb}}}$. Establishing a better relationship between d and ρ_{deb} is difficult because of the multiple ways in which these sessile segments can arrange and the different types of dislocations that can be locked in them. k_{deb} is a material-independent constant determined to be 0.086 (Madec et al., 2002).

3.3.6. Twin boundaries as barriers

If there are no twins in the crystal, τ^{s}_{HP} models the effect of grain size d_g via a Hall–Petch relationship $\sim K/\sqrt{d_g}$, where K is the Hall–Petch coefficient. In this case, τ^{s}_{HP} is the same for all $s \in \alpha$. Theoretical expressions for the coefficient based on microstructural phenomena, such as dislocation pile-ups, stress concentrations, or grain boundary sources, have been developed (Armstrong, 1968; Conrad, 1963; Meakin and Petch, 1963; Takeuchi, 1970; Li and Chou, 1970; Stroh, 1955). In these, the general forms are $K \sim f(\tau)\mu b$ or $f(\tau)\sqrt{\mu b}$, where f may include stress intensity factors, orientation dependencies, and fitting constants. In order to capture temperature dependence through μ, we adopt from these works the form:

$$\tau^{s}_{\text{HP}} = \mu \text{HP}^{\alpha}\sqrt{\frac{b^{\alpha}}{d_g}} \quad s \in \alpha \quad \text{without twins} \tag{3.21}$$

where $\mu\sqrt{b^{\alpha}}\text{HP}^{\alpha}$ is the Hall–Petch coefficient and HP^{α} is a dimensionless constant that depends on the type of slip dislocation α impinging on the grain boundary.

This microscale coefficient is not equivalent or even directly related to an analogous macroscale coefficient. In a number of Hall–Petch studies on hcp materials, typically a 'bulk average' coefficient is found and is observed to depend on strain and temperature (see Armstrong (1968) and Mannan and Rodriguez (1975) and references therein). Caution must be exercised when examining these results. Due to plastic anisotropy, the strong effect of texture, and the possibility of twinning in hcp materials, Hall–Petch coefficients obtained from bulk samples and monotonic loadings will vary substantially across studies in the literature. It is difficult to isolate changes in Hall–Petch effects with temperature and grain size, from changes in deformation mechanisms with temperature and grain size.

When there are twins present in the grain, τ^{s}_{HP} is different for each s. The mean free path d_{mfp} for slip system s is reduced and depends on the relative orientation of its slip plane and the predominant twin interface (Fig. 1). In this case, another 'Hall–Petch'-like coefficient $\text{HP}^{\alpha\beta}$ needs to be introduced to reflect the interactions particular to the type of slip α ($s \in \alpha$) and type of twin boundary of the PTS in the grain, (PTS $\in \beta$):

$$\tau^{s}_{HP} = \mu \mathrm{HP}^{\alpha\beta} \sqrt{\frac{b^{\alpha}}{d^{s,\mathrm{PTS}}_{mfp}}} \quad s \in \alpha \quad \text{with a } \beta\text{-type PTS} \tag{3.22}$$

3.3.7. Evolution of slip resistance

The slip resistance τ^{s}_{c} will evolve with straining from a zero-strain value, calculated from Eq. (3.16) to be:

$$\tau^{s}_{c}(\gamma = 0) = \tau^{\alpha}_{0}(T) + \mu \mathrm{HP}^{\alpha} \sqrt{\frac{b^{\alpha}}{d_{g}}} + b^{\alpha}\chi\mu\sqrt{\rho^{\alpha}_{0}} \quad \forall s \in \alpha \tag{3.23}$$

assuming that no twins are present and that the initial amount of debris is negligible. $\tau^{s}_{c}(\gamma = 0)$ has a microstructure dependence due to the initial values of ρ^{α}_{0}, $\alpha = 1,2$, and grain size d_g. ρ^{α}_{0} are assigned values typical for an annealed state: $\rho^{\alpha}_{0} = 10^{5}1/m^{2}$, $\alpha = 1,2$. $\tau^{s}_{c}(\gamma = 0)$ also has a temperature dependence provided by μ and $\tau^{\alpha}_{0}(T)$.

The final expression for the slip resistance for each slip mode α is

$$\tau^{s}_{c} = \tau^{\alpha}_{0}(T) + \mu \mathrm{HP}^{\alpha\beta} \sqrt{\frac{b^{\alpha}}{d^{s,\mathrm{PTS}}_{mfp}}} + b^{\alpha}\chi\mu\left[\sqrt{\rho^{\alpha}} + \frac{k_{\mathrm{deb}}}{\chi}\sqrt{\rho_{\mathrm{deb}}}\log\left(\frac{1}{b^{\alpha}\sqrt{\rho_{\mathrm{deb}}}}\right)\right]$$
$$s \in \alpha \quad \text{and with a } \beta\text{-type PTS.} \tag{3.24}$$

3.4. Resistance to twin propagation

The pole-mechanism theory (Thompson and Millard, 1952; Yoo and Wei, 1966) for twin nucleation involves the splitting of perfect dislocations into partials. This maneuver requires large stresses of the type associated with localized stress concentrators, such as pile-ups at grain boundaries, triple junctions, and other defects, or with high strain rates where the elastic contribution to total strain is large. Irrespective if this particular mechanism operates, the local stress σ_{nuc} required to create sources for partial dislocations must be larger than that to move slip dislocations or twin partials. According to some theories, stresses to produce the zonal twin dislocations come from dislocation pile-ups (Westlake, 1961) or high stresses are needed to grow twin embryos (a nucleus of partials) to a critical size before a twin can propagate from it (Yoo and Lee, 1991; Chyung and Wei, 1967).

As mentioned in Section 3.1, our model assumes a twin resistance calculated in the model as a shear stress τ resolved in the twin direction and twin plane, which applies best to twin propagation and not to nucleation. For the propagation process, we describe a critical propagation resistance τ^{t}_{c} for twin system t in twin mode β, which is the sum of three terms:

$$\tau^{t}_{c} = \tau^{\beta}_{0} + \tau^{t}_{HP} + \tau^{\beta}_{slip} \quad t \in \beta \tag{3.25}$$

The first term, τ^{β}_{0} is the propagation resistance, without the effects of surrounding slip dislocations τ^{β}_{slip} and grain or twin boundaries τ^{t}_{HP}. When the local internal stress σ exceeds σ_{nuc}, propagation is facilitated and τ^{β}_{0} equals τ^{β}_{prop}, the propagation resistance for a fully nucleated twin. On the contrary when σ is less than σ_{nuc}, then twinning has not yet nucleated and τ^{β}_{0} equals a critically high value τ^{β}_{crit}. To sum, τ^{β}_{0} can range between τ^{β}_{crit} and τ^{β}_{prop},

depending on the probability $P(\sigma>\sigma_{\text{nuc}})$ that nucleation has occurred. The average value for τ_0^β is therefore

$$\tau_0^\beta = \tau_{\text{crit}} P(\sigma < \sigma_{\text{nuc}}) + \tau_{\text{prop}} P(\sigma > \sigma_{\text{nuc}}) = \tau_{\text{prop}}^\beta + (\tau_{\text{crit}}^\beta - \tau_{\text{prop}}^\beta) P(\sigma < \sigma_{\text{nuc}}) \tag{3.26}$$

where we used: $P(\sigma > \sigma_{\text{nuc}}) = 1 - P(\sigma<\sigma_{\text{nuc}})$. Calculating $P(\sigma < \sigma_{\text{nuc}})$ requires knowing the nucleation mechanism for each twin type, and the (elastic) stress σ involved, as determined by local defects, triple junctions, pile-ups, incompatibilities across grain boundaries, etc.

Previous experimental characterization of tensile twin evolution with strain (e.g. McCabe et al., 2007) suggests that nucleation is difficult unless there is sufficient accumulation of prismatic dislocations. Tensile $\{10\bar{1}2\}$ twin propagation seems to require much less stress than nucleation. Based on these observations, we assume that for tensile twins $\tau_{\text{crit}} \gg \tau_{\text{rop}}$, and the transition is mediated by prismatic dislocations, letting $P(\sigma < \sigma_{\text{nuc}}) = \exp(-\rho^1/\rho^1_{\text{sat}})$. For $\{11\bar{2}2\}$-twinning, on the other hand, single crystal c-axis compression experiments by Akhtar (1973b) suggest that the propagation stress is only slightly smaller than the nucleation stress. For compressive twins, we set $\tau_{\text{prop}} = \tau_{\text{crit}}$.

At this stage, we assume that τ_0^β is temperature and strain rate independent. It is unclear, however, if and how τ_0^β depends on these conditions because twinning rarely occurs in polycrystalline Zr in isolation, that is, without the influence of slip. Often times, frequent twinning at low temperatures and/or high strain rates could be explained by a concomitant difficulty for slip under these conditions. On the other side, it is possible to isolate twinning in molecular mechanics simulations (Serra et al., 1991). Such calculations on hypothetical hcp crystals show that for some twin Burgers vectors, additional atomic shuffles are required to place the lattice in twin orientations. Energy from stress and/or temperature would be required to move the remaining atoms into twin orientation. $\{11\bar{2}2\}$-twinning for example is found to require more complex shuffles than $\{10\bar{1}2\}$-twinning. This would imply that $\tau_0^{\beta=2}$ for $\{11\bar{2}2\}$-twin propagation may exhibit sensitivity to temperature. Later in Section 5 we return to this issue[1].

We also include a Hall–Petch term $\tau^{\text{t}}_{\text{HP}}$ for grain size effect or barrier effect due to the predominant twin system (PTS) within the grain.

$$\tau^{\text{t}}_{\text{HP}} = \frac{\text{HP}^\beta}{\sqrt{d_{\text{g}}}} \quad \text{with no twins or when } t \in \beta \quad \text{and} \quad t = \text{PTS} \tag{3.27a}$$

$$\tau^{\text{t}}_{\text{HP}} = \frac{\text{HP}^{\beta\beta'}_{\text{TW}}}{\sqrt{d^{\text{s}}_{\text{mfp}}}} \quad \text{when } t \in \beta,\ \ t \neq \text{PTS}, \text{PTS} \in \beta' \tag{3.27b}$$

The superscript β reflects the type of twin, e.g. $\beta = 1$ for $\{10\bar{1}2\}$-twinning or $\beta = 2$ for $\{11\bar{2}2\}$-twinning. The other superscript β' reflects the mode of the PTS in the grain, which may or may not be the same system as β. Note that unlike the HP^α term for slip, based on dislocation pile-ups, the Hall–Petch coefficients for twins are not based on any physical model. These empirical constants have dimensions, stress $\cdot\sqrt{length}$.

We have verified that assuming $\tau_{\text{c}}^\beta = \tau_0^\beta + \tau^{\text{t}}_{\text{HP}}$ alone does not predict the observed hardening in the flow stress of Zr in the range of temperatures when twinning is prevalent ($T < 150$ K). While the Hall–Petch term introduces hardening through the evolution of

[1] No doubt will the twin nucleation process, not treated here, be sensitive to strain rate and temperature. Both twin nucleation and strain rate effects are beyond the scope of this work.

$d_{mfp} < d_g$ for twins $t \in \beta$, $t \neq$ PTS, it does not provide hardening for the PTS, Eq. (27). Because twinning dislocations of the PTS are often the most active twin dislocations in the crystal and responsible for twin growth, neglecting hardening in their propagation resistance can lead to inaccurate predictions. The purpose of the last term in Eq. (3.25), τ^{β}_{slip}, is to contribute hardening for all twin systems due to interactions with slip dislocations. τ^{β}_{slip} can grow proportionally with the slip dislocation population:

$$\tau^{\beta}_{slip} = \mu \sum_{\alpha} C^{\beta\alpha} b^{\beta} b^{\alpha} \rho^{\alpha} \tag{3.28}$$

where b^{β} is the magnitude of the Burgers vector for the zonal twinning dislocation (Yoo and Loh, 1970; Partridge, 1967). τ^{β}_{slip} provides temperature- and strain-rate-dependent hardening for twin propagation τ^{β}_{c} that depends on both slip type α and twin type β. Slip dislocations can either promote or hinder twin propagation. We consider the more frequent event that $C^{\beta\alpha} > 0$; in other words, accumulation of slip dislocations retards and eventually suppresses twin growth (Boucher and Christian, 1972; Mahajan and Williams, 1973; Song and Gray, 1995a,b), acting as obstacles for the passage of twinning dislocations. However there are special cases (see Section 6) in which slip dislocations can aid zonal twin generation and propagation, $C^{\beta\alpha} < 0$. Interactions between twinning and the debris population are found to be negligible.

4. Experimental procedure

The material used in this work is of the same clock-rolled plate that was used in our previous studies of Zr (Tomé et al., 2001; Kaschner et al., 2006). The material was acquired as high-purity crystal bar Zr (<100 ppm). The crystal bar was vacuum arc-melted, cast into an ingot, and then processed by knockdown forging followed by several passes through a rolling mill at room temperature. The final product is a clock-rolled plate with a strong axisymmetric texture, as shown in Fig. 3. After an anneal at 550 °C for 1 h, the grains are free of twins, equiaxed, and have an average diameter of approximately 15–20 μm. Sample preparation and testing procedures are detailed in Beyerlein et al. (2007).

5. Results

Fig. 4a–c shows the stress–strain response at four different temperatures in (a) IPT (1-direction), (b) IPC (1-direction), and (c) TTC (3-direction) (Beyerlein et al., 2007). The anisotropy does not change with temperature; at all temperatures TTC requires to deform the aggregate along the hard c-axis and leads to the highest flow stress. IPC is the next

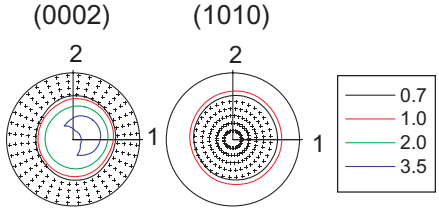

Fig. 3. Basal (0002) and prism (10.0) pole figures for the initial annealed Zr studied here.

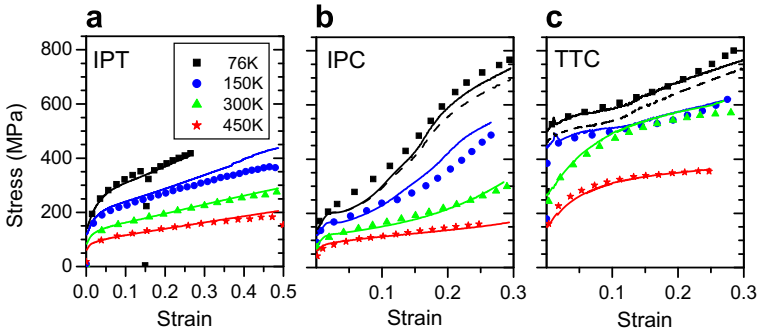

Fig. 4. Flow response of zirconium at four temperatures for (a) in-plane tension, (b) in-plane compression and (c) through-thickness compression (see Fig. 3 for coordinates). Measured responses are the symbols and model predictions are the solid lines, using the parameters listed in Tables 2 and 3. The dashed line corresponds to assuming that the propagation stress for $\{11\bar{2}2\}$ compressive twinning is constant ($\tau_0 = 300$ MPa).

highest, and IPT, the lowest. Fig. 4 also includes the results of the model using the parameters listed in Tables 2 and 3. The calculated basal and prism pole figures corresponding to 25% strain are shown in Fig. 5 for all the cases. The relative activity (percent contribution to total shear rate) of prism slip, pyramidal slip, tensile twins and compressive twins within the matrix and the twin domains, is reported in Fig. 6 as a function of strain.

Table 2
Hardening parameters for slip in stages II–IV

	$\alpha = 1$ Prismatic	$\alpha = 2$ Pyramidal $\langle c + a \rangle$	
k_1^α	1.25E + 08 m	2.25E + 10 m	
$\dot{\varepsilon}_0^\alpha$	10^7 1/s	10^7 1/s	
g^α	3.75E − 03	3.2E − 02	
D_0^α	330 MPa	100 MPa	
A^α	37 $(1 + T/30\ \mathrm{K})$	0.1	
τ_0^α	40.8 $\exp\left(-\frac{T}{305\ K}\right)$ MPa	722.5 $\exp\left(-\frac{T}{200\ K}\right)$ MPa	
χ	0.9	0.9	
q	4	4	
HP^α	100	170	
$HP^{\alpha\beta}$	100	N/A[a]	$\beta = 1, \{10\bar{1}2\}$ Twinning
	250	N/A	$\beta = 2, \{11\bar{2}2\}$ Twinning

[a] N/A indicates that the parameter was not needed and therefore it could not be characterized.

Table 3
Parameters for twinning

	$\beta = 1$, tensile twinning	$\beta = 2$, compressive twinning	
τ_0^β	$\tau_{crit} = 165$ MPa, $\tau_{prop} = 20$ MPa	$\tau_{crit} = \tau_{prop} = 300 + 569 \exp\left(-\frac{T}{28.6\ K}\right)$ MPa[b]	
HP^β	35 MPa $m^{1/2}$	100 MPa $m^{1/2}$	
$HP_{TW}^{\beta\beta'}$	35 MPa $m^{1/2}$	100 MPa $m^{1/2}$	
$C^{\beta\alpha}$	N/A[a]	8000	$\alpha = 1$ (prismatic)
	N/A	600	$\alpha = 2$ (pyramidal)

[a] N/A indicates that the parameter was not needed and therefore it could not be characterized.
[b] See text in Section 5.3.

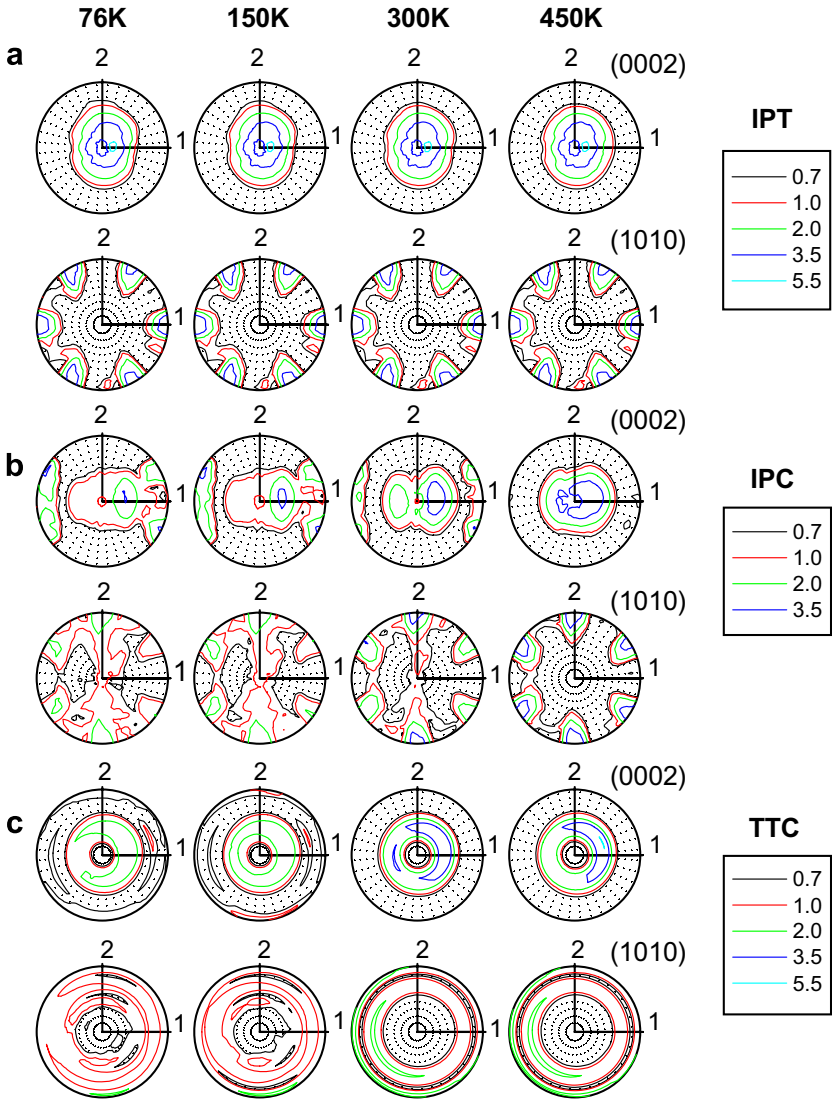

Fig. 5. Predicted basal (0002) and prism (10.0) pole figures at four temperatures after 0.25 straining for (a) in-plane tension, (b) in-plane compression and (c) through-thickness compression (see Fig. 3 for coordinates).

5.1. In-plane tension

The experimental IPT curves (Fig. 4a) lack the increasing hardening rate characteristic of twinning activity. In addition, our simulations indicate that at all temperatures IPT deformation is overwhelmingly accommodated by prismatic slip and for this reason we omit reporting relative activity in Fig. 6 for this case. The final texture is also consistent with prismatic activity: no reorientation of the basal poles and an alignment of the (1 0 1 0) poles with the tensile direction (Fig. 5). The conventional laws for temperature

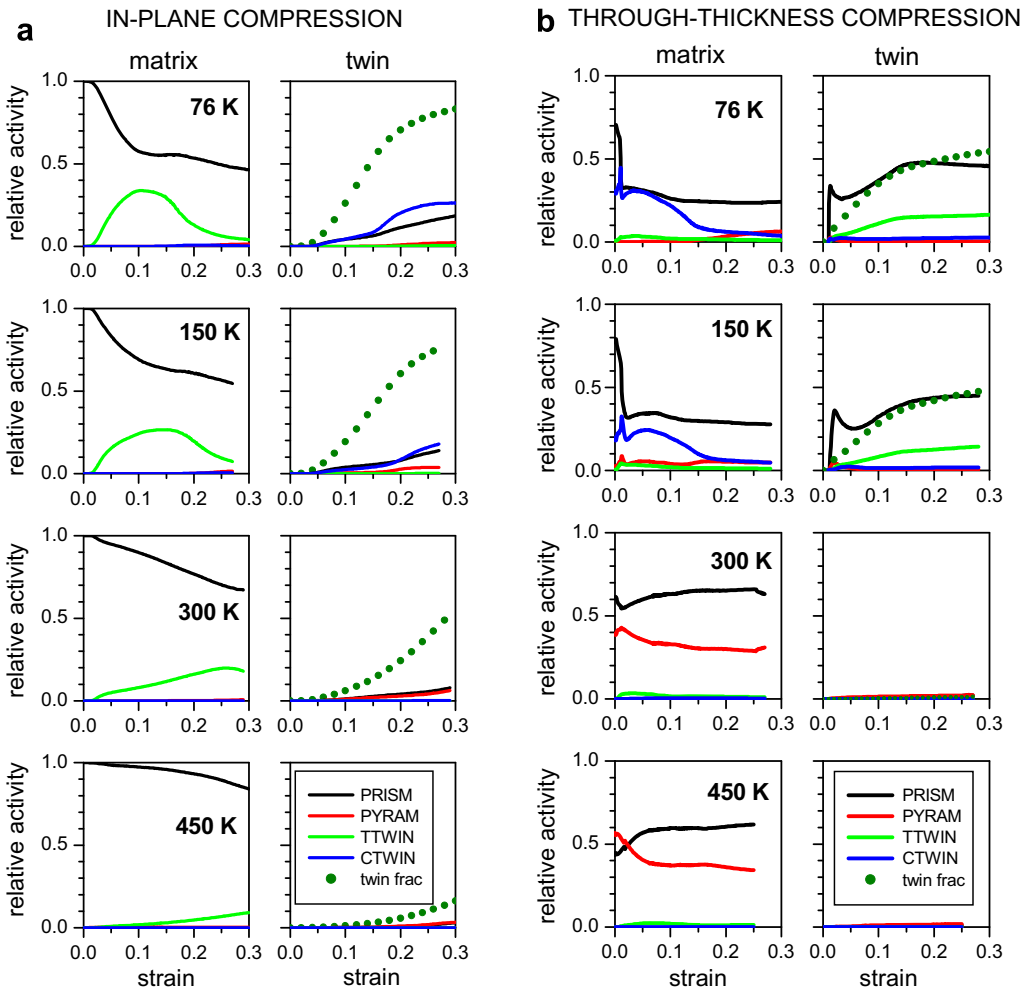

Fig. 6. Predicted relative contribution of slip and twinning to strain, inside the matrix and twin domains of the Composite Grain, at four temperatures: (a) in-plane compression and (b) through-thickness compression.

effects, as established for fcc materials, hold in this case: the stage II hardening rate is insensitive to temperature, the stage III transition stress increases inversely with temperature, and the stage IV hardening rate only increases slightly as temperature decreases. This same result has also been observed in Zr single crystals oriented for prismatic slip (Akhtar and Teghtsoonian, 1971).

5.2. In-plane compression

In IPC noticeable transitions in hardening are observed as the temperature decreases from 450 K to 76 K. According to the model calculations this transition can be correlated

with a transition from prismatic slip-dominated deformation at 450 K, to an increasing amount of tensile twin activity as the temperature decreases (see Fig. 6). Correspondingly, an increasing twin volume fraction is predicted (up to 80% at 76 K), as well as an increasing prismatic plus compressive twin activity inside the tensile twins. When twinning is active, the strain hardening rate increases due to the Hall–Petch effect. Because of twinning, the IPC flow response does not follow the conventional stages of work hardening.

In addition to temperature, deformation mechanisms can also change with strain level. At small strains (and for most of straining at 450 K), the IPC and IPT tests have the same flow response, which indicates that the same slip mechanism is active in both cases. The deviation between the IPC and IPT curves with further straining signify the onset of tensile twinning. Tensile twinning is activated by IPC but not by IPT; hence, the compression strength begins to exceed the tension strength after the onset of twinning (compare Fig. 4a and b). Model interpretations (Fig. 6) suggest that $\{10\bar{1}2\}$ twins require some amount of prismatic dislocation accumulation prior to propagation. At high strains, they also show that $\{10\bar{1}2\}$ twinning saturates because further nucleation or further propagation is impeded by deformation microstructure or secondary twinning. Consequently, for 76 K and 150 K, the IPC flow response contains well-defined inflection points marking changes in activity from slip to tensile twinning and then to secondary compressive twinning within the tensile twins (Fig. 6a). As shown in Fig. 5b, the textures change with temperature accordingly: predominant prism slip aligns the compression axis with the $(11\bar{2}0)$ direction and leaves the basal poles invariant (450 K). Tensile twinning activity induces a re-orientation of the basal poles along the compression axis (in this case along the 1-direction).

5.3. Through-thickness compression

In TTC a sharp transition in hardening takes place between room temperature and 150 K. The model calculations indicate that at and above room temperature prismatic and pyramidal slip prevail (Fig. 6c), leading to a decreasing hardening rate. Below 300 K, the hardening rate increases with strain indicating increasing compression twin activity. This transition between 300 K and 150 K has to do with a change in deformation mechanism from pyramidal slip to $\{11\bar{2}2\}$-twinning (Fig. 6c). The model agreement suggests that the transition is due to an extreme sensitivity in the initial pyramidal slip resistance τ_0^2 to temperature, dramatically increasing with decreasing temperature. Consequently, at low temperatures pyramidal slip is completely suppressed and replaced by $\{11\bar{2}2\}$-twinning. Because of this, we cannot estimate τ_0^2 for pyramidal slip at temperatures below 150 K, but rather provide a lower bound for it (see Eq. (3.18) and Fig. 2). The texture evolves slowly at room temperature and higher, but at 150 K and lower, compressive twinning has re-oriented the *c*-axis to the outer rim (Fig. 5c). As shown in Fig. 6c, prismatic slip is expected to be very active inside the compressive twins and some tensile twin activity is also predicted.

Calculations in Fig. 4 assume that tensile and compressive twinning is temperature independent. Agreement can be improved markedly if these modes were made temperature dependent. For instance, in Section 3.4 it is argued that compressive twinning may vary inversely with T. If we increase $\tau_0^{\beta=2}$ in Eq. (3.26) from 303 MPa to 340 MPa as the temperature decreases from 150 K to 76 K, the model more effectively predicts the flow response at 76 K in all three directions (see dashed line in Fig. 4). This adjustment

corresponds to $\tau_0^{\beta=2}$ in Eq. (3.26) continuously increasing with decreasing temperature within $T \geq 76$ K according to $\tau_0^{\beta=2} = \tau_{\text{prop}} = \tau_{\text{crit}} = 300 + 569\exp(-T/28.6\,K)$ MPa. This expression is compared with the initial strength of the other modes in Fig. 2.

5.4. Implications for prismatic $\langle a \rangle$ and pyramidal $\langle c + a \rangle$ slip

Agreement with all IPT tests and the TTC tests at and above 300K provides estimates for the thermal activation parameters for prismatic and pyramidal slip. We find that $D_0^{\alpha} = 330$ MPa and $g^{\alpha} = 3.75\text{E}-03$ for prismatic, and $D_0^{\alpha} = 100$ MPa, $g^{\alpha} = 0.032$ for pyramidal. The higher D_0^{α} means that prismatic glide is more sensitive to stress than pyramidal glide. The g^{α} for pyramidal is an order of magnitude greater than that for prismatic indicating that, as expected, pyramidal slip is the harder slip mode. For modeling stage IV, we introduce an expression for the fraction of dislocations that are converted to debris equation (3.14). The fraction is two orders of magnitude higher for prismatic slip than pyramidal slip and, unlike pyramidal slip, is sensitive to temperature. This suggests a higher rate of debris formation for prismatic slip than pyramidal $\langle c + a \rangle$. Stable substructure found in pure Zr for orientations and temperatures in which slip prevails over twinning would consist mainly of prismatic dislocations. Akhtar and Teghtsoonian (1971) show that Zr crystals deforming in prismatic slip at 78 K have qualitatively similar microstructure development as in fcc materials, from long intersecting screw dislocations in stage II to braids and cellular structures well into stage III.

6. Discussion and conclusions

We present here a dislocation-based temperature-dependent constitutive model for Zr. Separate hardening laws for each slip and twinning mode are introduced, with their own temperature (and rate) sensitivities. As each grain orientation deforms by multiple mechanisms, proper treatment of their interactions is necessary. Developing the formulation within a crystallographic framework allows coupling between crystal orientation, slip resistance, twin re-orientation, and twin propagation. We justify the inclusion of different terms in the hardening laws and their functional dependence with stress, temperature and rate. We have tried to minimize the number of parameters and, when possible, isolated specific mechanisms described by those parameters. We are confident that this formulation will describe reliably quasi-static deformation rates within the temperature range 76–450 K.

We would like to devote the remainder of this Section to discuss some of our model assumptions and potential extensions. In forthcoming studies, we plan to perform a systematic testing program that characterizes hardening, twin fraction and texture evolution associated with changes in strain path, testing temperature, and strain rate. Such non-homogeneous testing will be designed to enhance the role of specific mechanisms (e.g. interaction of prism slip with compressive twins), and will further test the model.

6.1. Selection of deformation modes

In the quasi-static strain rate $10^{-3}\,\text{s}^{-1}$ and temperature regimes studied here, the temperature-dependent response and anisotropy of pure polycrystalline Zr could be

modeled using thermal-activation controlled slip for prismatic and pyramidal $\langle c+a\rangle$ dislocations and two twinning modes, tensile twinning $\{10\bar{1}2\}(10\bar{1}\bar{1})$, and compressive twinning $\{11\bar{2}2\}(11\bar{2}\bar{3})$. Other modes, such as pyramidal $\langle a\rangle$ and $\{11\bar{2}1\}(11\bar{2}\bar{6})$ tensile twins have been observed (McCabe et al., 2007) but they do not seem to contribute substantial shear. Recent interpretations of Zr textures after severe plastic deformation by ECAE (100% simple shearing) at room temperature suggest that substantial amounts of basal slip act along with prismatic during the extrusion (Yu et al., 2005; Yapici et al., in press; Perlovich et al., 2005). While in single crystals basal slip has been observed at high temperatures (850 K) (Akhtar, 1973a,b) or in the vicinity of twins and some preferentially oriented grains at room temperature (Martin and Reed-Hill, 1964; Dickson and Robin, 1973; Dickson and Craig, 1971), it is possible in ECAE that locally high stresses due to high dislocation densities generated at large strains, or at subgrain boundaries (reduction in effective grain size) promoted basal activity.

6.2. Role of substructure

The relationship between the evolution of dislocation density, substructure formation, and macroscopic workhardening under large strains (stages III and IV) is still poorly understood. In fcc materials, the microstructure evolves from homogeneous to being more localized with strain and a well-defined substructure in the form of kink- and micro-bands, cells, sheet-like subboundaries develops by stages III and IV (Mader, 1963; Haasen, 1989; Swann, 1963). Most models that relate microstructure to workhardening have been exclusively developed for cubics (Estrin and Mecking, 1984; Estrin et al., 1998; Kubin and Estrin, 1990; Klepaczko, 1991; Busso and McClintock, 1996; Kok et al., 2002; Peeters et al., 2001; Mahesh et al., 2004; Pontes et al., 2006; Beyerlein and Tomé, 2007). Some of these consider the dislocation populations assembled in the substructure to have a different behavior than those found elsewhere in the grain, such as forest dislocations found in the interior of cells, subgrains, or grains (Estrin et al., 1998; Klepaczko, 1991; Peeters et al., 2001; Mahesh et al., 2004) or include additional terms in the dislocation rate equations for a constant (Estrin and Mecking, 1984; Fernandes and Vieira, 2000) or evolving mean free path (Kok et al., 2002). Furthermore dislocations found in the cell walls are assumed to behave differently than those found in sheet-like sub-boundaries. In this model, stage IV is simply attributed to an increase of debris storage, without specific regard to where in the microstructure (i.e., within, near, or far from cell walls, subboundaries, grain boundaries) debris formation operates. Our model is uniquely formulated to extract debris from recovery processes and have it contribute to stage IV hardening.

Before considering more formal treatments of substructure evolution, our understanding of twin nucleation and propagation must be improved. In hcp materials twinning is more prevalent than in fcc materials. Twinning affects the macroscopic hardening in such a way that the usual workhardening stages from slip, like stages III and IV, may not be observed. Our findings suggest that in the presence of substantial twinning, substructure or debris storage has little influence on hardening compared to the directional barrier effect of twin boundaries. Directional barrier effects of subboundaries (like GNDs) may well start contributing once the twinning structure is fully developed, which would occur at strain levels beyond those tested here.

6.3. Coupling between slip modes

In an hcp crystal where it is possible that many slip modes can act simultaneously, the deformation behavior will not only be the result of interactions between dislocation of the same type α, but also of those between dislocations of different types. Thus far in our development and application of the model, coupling has only been introduced, albeit unavoidably, in the development for the rate of debris formation. In spite of the distinct roles assigned to each rate term in Eq. (3.6) and to each population ρ^{α} and ρ_{deb}, the rate equations and slip resistance models are still simplifications of the actual dynamical dislocation processes and for the most part neglect any possible coupling between the different dislocation populations. For completeness, model extensions for coupling between distinct dislocation populations are suggested. There are two possible areas in which coupling can be introduced in the model. The first way is through dislocation-density evolution, and the second way is through the evolution of slip resistance.

In the first, for example, it is possible that ρ_{deb} can increase the rate of dislocation multiplication, such as by introducing new Frank-Read sources. In this case, the generation rate expression for populations ρ^{α} could contain a term dependent on ρ_{deb}. Also interactions between moving dislocations and debris can create more debris by altering the configuration of the dislocation or forcing segments out of their glide plane. In this case, the rate expression for debris would contain a term dependent on populations ρ^{α}. Last one can couple the density evolution of one type of slip dislocation population α, say prismatic slip, to the activity of another type α', say pyramidal or basal slip, by introducing interaction parameters $h^{\alpha\alpha'}$.

$$\frac{\partial \rho^{\alpha}}{\partial \gamma^{\alpha}} = k_1^{\alpha}\sqrt{\hat{\rho}^{\alpha}} - k_2^{\alpha}\hat{\rho}^{\alpha} \tag{6.1}$$

where

$$\hat{\rho}^{\alpha} = h^{\alpha\alpha\prime}\rho^{\alpha\prime} \tag{6.2}$$

This modification allows for the active slip modes to couple and contribute to the generation or annihilation of each other.

In the second, forest dislocations from one population α are made to contribute to the slip resistance for gliding dislocations in the other α', by introducing a separate set of interaction parameters, $g^{\alpha\alpha'}$. Forest dislocations cutting any given slip plane can consist of any type of dislocation, e.g. prismatic and pyramidal $\langle c+a\rangle$. Using $g^{\alpha\alpha'}$, we re-write the forest contribution to slip resistance as:

$$\tau_{\text{forest}}^{\alpha} = b^{\alpha}\chi\mu\sqrt{g^{\alpha\alpha\prime}\rho^{\alpha'}} \tag{6.3}$$

The influence of interactions between distinct populations of slip dislocations is reflected by the off-diagonal components of $g^{\alpha\alpha'}$. Suppose for example that $g^{\alpha\alpha'} = 1$ when $\alpha = \alpha'$. Then $g^{\alpha\alpha'} = 0$, $\alpha \neq \alpha'$ means that only α-type dislocation contribute to hardening on α slip planes. On the other hand, $g^{\alpha\alpha'} > 1$, $\alpha \neq \alpha'$ means that dislocations α' of different type contribute more to the slip resistance for gliding α-dislocations than α dislocations.

6.4. Coupling between slip and twinning modes

Several key features of the model highlight important interactions between slip and twinning. First, the assumption is made that twin boundaries are impenetrable to slip, and a Hall–Petch model is applicable, with the appropriate twin spacing in place of grain

size. This assumption is likely not to apply in all interactions between approaching slip dislocations and twin barriers. For instance, Yoo (1969) shows that it is possible for prismatic (and basal) screw dislocations to cross-slip onto tensile twins $\{1\,0\,\bar{1}\,2\}$ when the dislocation line is parallel to the line of intersection between the twin plane and slip plane. In this case, a Hall–Petch-like effect would not take place for prismatic dislocations that cross-slip onto the $\{1\,0\,\bar{1}\,2\}$-interface. As support, prismatic slip dislocations have been observed in $\{1\,0\,\bar{1}\,2\}$ twinned regions (Akhtar and Teghtsoonian, 1971) and evidence of this cross-slip mechanism is provided in (Dickson and Robin, 1973). Second, agreement with our model in Eq. (3.26) suggests that mechanisms for activating tensile twinning need a sufficient amount of prismatic dislocation accumulation. Last, coupling between slip and twinning is entered in the model via the coupling parameter $C^{\beta\alpha}$ in Eq. (3.28). In this application, we find that $C^{\beta\alpha} > 0$, and accordingly after the twinning dislocations have nucleated, slip dislocations α contribute to the work hardening of τ_c^t for all twin systems, $t \in \beta$, $\beta = 1,2$. On the contrary, there is some experimental evidence that prismatic dislocations can aid twin propagation, rather than hinder it (Song and Gray, 1995a,b; Dickson and Robin, 1973). Song and Gray (1995a,b) and Dickson and Robin (1973) show that the matrix and twin regions immediately on either side of the $\{1\,0\,\bar{1}\,2\}$ twin boundary must locally deform by prismatic slip (Dickson and Robin, 1973) in order to accommodate twin boundary movement. Moreover using geometrical arguments, Yoo (1969) shows that zonal twin dislocations needed for growth can be generated when (edge) prismatic dislocations react with a $\{1\,0\,\bar{1}\,2\}$ boundary.

Agreement would improve of course if these mechanisms for slip–twin interactions were made temperature-dependent in the model, but this is not attempted here. For example, although the coupling parameters $C^{\beta\alpha}$ are not explicit functions of T in this work, there is no reason they should not be. It is quite possible that T can alter the way slip and twin dislocations interact.

6.5. Rate effects

Although strain rate enters into part of the formulation, it is not explored in this work. Specifically, model parameters have been characterized at $10^{-3}\ s^{-1}$ only. In future work, the model developed here will be used to study rate-effects for rates in the range $10^{-3}\ s^{-1}$ to $10^{3}\ s^{-1}$. At higher rates of strain ($>10^{4}\ s^{-1}$), the model does not apply as thermal activation may no longer control the rate of deformation. Because the stresses can grow to be quite large, especially in short-range, close to twin and dislocation boundaries, dislocation motion no longer depends on the energy supplied by thermal fluctuations. Dislocation inertia takes effect such that dislocations possess kinetic energy which can be used to overcome obstacles and repulsive interactions with other dislocations, e.g. (Wang et al., 2007). Dislocation velocities tend toward a linear relationship with stress rather than an exponential one (see Section 3.2.4). Also, at higher rates twinning is more active and grains may contain sets of intersecting twins (Song and Gray, 1995a,b).

Acknowledgements

Support by Office of Basic Energy Sciences Project FWP 06SCPE401 is gratefully acknowledged. The authors are grateful to G. Kaschner and M. Lovato for allowing us to use their mechanical test data at 150 K and 450 K prior to publication.

References

Akhtar, A., 1973a. Basal slip in zirconium. Acta Metall. 21, 1–11.

Akhtar, A., 1973b. Compression of zirconium single crystals parallel to the *c*-axis. J. Nuc. Mat. 47, 79–86.

Akhtar, A., 1975. Prismatic slip in zirconium single crystals at elevated temperatures. Met. Trans. 6A, 1217–1221.

Akhtar, A., 1976. Pyramidal slip in cobalt. Scripta Metall. 10, 365–366.

Akhtar, A., Teghtsoonian, A., 1971. Plastic deformation of zirconium single crystals. Acta Metall. 19, 655–663.

Argon, A.S., Haasen, P., 1993. A new mechanism of work-hardening in the late stages of large-strain plastic-flow in fcc and diamond cubic-crystals. Acta Metall. 41, 3289–3306.

Armstrong, R.W., 1968. Theory of the tensile ductile-brittle transition behavior of polycrystalline h.c.p. materials, with application to beryllium. Acta Metall. 16, 347–355.

Becker, R., 1925. On the plasticity of amorphous and crystalline solids. Phys. Z. 26, 919–925.

Beyerlein, I.J., Tomé, C.N., 2007. Modeling transients in the mechanical response of copper due to strain path changes. Int. J. Plasticity 23, 640–664.

Beyerlein, I.J., Kaschner, G.C., Tomé, C.N., 2007. Plastic anisotropy of pure zirconium at 76 K to 450 K. In: Proceedings of Plasticity 2007, Alaska, June 2–7, 2007. CD-ROM.

Blish, R.C., Freeland Jr., T., 1969. Dislocation velocity on the $\{\bar{1}2\bar{1}2\}\langle 1\bar{2}13\rangle$ slip system of zinc. J. Appl Phys. 40, 884–890.

Boucher, N.A., Christian, J.W., 1972. The influence of pre-strain on deformation twinning in niobium single crystals. Acta Metall. 20, 581–591.

Burgers, W.G., 1940. Plasticity of crystals. In: Houwink, R. (Ed.), Elasticity, Plasticity, and Structure of Matter. Cambridge University Press, London, pp. 73–127.

Busso, E.P., McClintock, F.A., 1996. Dislocation mechanics-based crystallographic model of a B2-type intermetallic alloy. Int. J. Plasticity 12, 1–28.

Cazacu, O., Plunkett, B., Barlat, F., 2006. Orthotropic yield criterion for hexagonal closed packed metals. Int. J. Plasticity 22, 1171–1194.

Chen, S.R., Gray III, G.T., 1997. Influence of twinning on the constitutive responses of Zr: experiments and modeling. J. Phys. IV France 7, C3-741–C3-746.

Chyung, C.K., Wei, C.T., 1967. Nucleation of deformation twins in zinc bicrystals. Phil. Mag. 15, 161–175.

Conrad, H., 1963. Electron Microscopy and Strength of Crystals. John Wiley and Sons, NY, pp. 299.

Dai, Y., Victoria, M., 1997. Defect structures in deformed F.C.C. metals. Acta Mater. 45, 3495–3501.

Dickson, J.I., Craig, G.B., 1971. Room temperature basal slip in zirconium. J. Nuc. Mat. 40, 346–348.

Dickson, J.I., Robin, C., 1973. The incorporation of slip dislocations in $\{1\bar{1}02\}$ twins in zirconium. Mat. Sci. Eng. 11, 299–302.

Dorn, J.E., Mitchell, J.B., 1964. Slip mechanisms in single crystals of hexagonal close-packed phases. In: High-Strength Materials, Proceedings of the Second High-Strength Materials – Berkeley International Materials Conference, pp. 510–577 (Chapter 12).

Dunlop, J.W., Brechet, Y.J., Legras, L., Estrin, Y., 2006. Dislocation density-based modelling of plastic deformation of Zircaloy-4. Mater. Sci. Eng. A 443, 77–86.

Essmann, U., Mughrabi, H., 1979. Annihilation of dislocations during tensile and cyclic deformation and limits of dislocation densities. Phil. Mag. A 40, 731–756.

Estrin, Y., Mecking, H., 1984. A unified phenomenological description of work hardening and creep based on one-parameter models. Acta Metall. 32, 57–70.

Estrin, Y., Toth, L.S., Molinari, A., Brechet, Y., 1998. Dislocation-based model for all hardening stages in large strain deformation. Acta Mater. 46, 5509–5522.

Eyring, H., 1936. Viscosity, plasticity, and diffusion as examples of absolute reaction rates. J. Chem. Phys. 4, 283–291.

Fernandes, J.V., Vieira, M.F., 2000. Further development of the hybrid model for polycrystal deformation. Acta Mater. 48, 1919–1930.

Fisher, E.S., Renken, C.J., 1964. Single-crystal elastic moduli and the hcp to bcc transformation in Ti, Zr, and Hf. Phys. Rev. 135, A482–A494.

Flynn, P.W., Mote, J., Dorn, J.E., 1961. On the thermally activated mechanism of prismatic slip in magnesium single crystals. Trans. Metal Soc. AIME 221, 1148–1154.

Follansbee, P.S., Kocks, U.F., 1988. A constitutive description of the deformation of copper based on the use of the mechanical threshold stress as an internal state variable. Acta Metall. 36, 81–93.

Friedel, J., 1959. Internal Stresses and Fatigue in Metals. Elsevier, Amsterdam, pp. 220.

Friedel, J., 1963. On the elastic limit of crystals. Electron Microscopy and Strength of Crystals. John Wiley and Sons, NY, pp. 605–648.
Garber, R.I., Gindin, I.A., Yu, U., Shubin, V., 1963. Slipping of beryllium single crystals along the hexagonal axis in the temperature range, 4.2–900 K. Soviet Phys. Solid State 5, 315–320.
Gilman, J.J., 1969. Micromechanics of Flow in Solids. McGraw-Hill Book Company, New York.
Gilman, J.J., 2002. Toward physically-based rate laws for dislocations. Mater. Sci. Eng. A 322, 126–131.
Haasen, P.J., 1989. A cell theory for stage IV work hardening of metals and semiconductors. Physique 50, 2445–2454.
Hirsch, P.B., 1959. Internal Stresses and Fatigue in Metals. Elsevier, Amsterdam, p. 139.
Hirth, J.P., Lothe, J., 1982. Theory of Dislocations. John Wiley and Sons, New York.
Kaschner, G.C., Tomé, C.N., Beyerlein, I.J., Vogel, S.C., Brown, D.W., McCabe, R.J., 2006. Role of twinning in the hardening response of zirconium during temperature reloads. Acta Mater. 54, 2887–2896.
Klepaczko, J.R., 1991. Physical-state variables – the key to constitutive modeling in dynamic plasticity. Nuc. Eng. Des. 127, 103–115.
Kocks, U.F., Mecking, H., 2003. Physics and phenomenology of strain hardening: the FCC case. Prog. Mater. Sci. 48, 171–273.
Kocks, U.F., Rollett, A.D., 1994. A review of the stages of work hardening. Solid State Phen., 1–18.
Kocks, U.F., Argon, A.S., Ashby, M.F., 1975. Thermodynamics and kinetics of slip. Prog. Mat. Sci. 19, 1–281.
Kok, S., Beaudoin, A.J., Tortorelli, D.A., 2002. Continuum approach to stage IV hardening. Acta Mater. 50, 1653–1667.
Kubin, L.P., Estrin, Y., 1990. Evolution for dislocation densities and the critical conditions for the Portevin-LeChatelier effect. Acta Metall. Mater. 38, 697–708.
Kuhlmann, D., 1951. On the theory of plastic deformation. Phy. Soc. Proc. 64, 140–155.
Langford, G., Cohen, M., 1969. Strain hardening of iron by severe plastic deformation. Trans. ASM 62, 623–638.
Lavrentev, F.F., 1980. The type of dislocation interaction as the factor determining work hardening. Mater. Sci. Eng. 46, 191–208.
Lebensohn, R.A., Tomé, C.N., 1993. Self-consistent anisotropic approach for the simulation of plastic deformation and texture development of polycrystals: application to zirconium alloys. Acta Metall. Mater. 41, 2611–2624.
Li, J.C.M., Chou, Y.T., 1970. Role of dislocations in the flow stress grain size relationships. Met. Trans. 1, 1145–1159.
Madec, R., Devincre, B., Kubin, L.P., 2002. From dislocation junctions to forest hardening. Phys. Rev. Lett. 89, 255508-1–255508-4.
Mader, S., 1963. Surface and thin-foil observations of the substructure in deformed fcc and hcp metal single crystals. Electron Microscopy and Strength of Crystals. John Wiley and Sons, New York, pp. 183–229 (Chapter 4).
Mahajan, S., Williams, D.F., 1973. Deformation twinning in metals and alloys. Int. Metall. Rev. 18, 43–61.
Mahesh, S., Tomé, C.N., McCabe, R.J., Kaschner, G.C., Beyerlein, I.J., Misra, A., 2004. Application of a substructure-based hardening model to copper under loading path changes. Metall. Mater. Trans. A 35, 3763–3774.
Mannan, S.L., Rodriguez, P., 1975. Grain size dependence of the deformation behavior of cadmium. Acta Metall. 23, 221–228.
Martin, J.L., Reed-Hill, R.E., 1964. A study of basal slip kink bands in polycrystalline zirconium. Trans. Metal Soc. AIME 230, 780–785.
McCabe, R.J., Cerreta, E.K., Misra, A., Kaschner, G.C., Tomé, C.N., 2007. Effects of texture, temperature and strain on the deformation modes of zirconium. Phil. Mag. A86, 3595–3611.
Meakin, J.D., Petch, N.J., 1963. Symposium on the Role of Substructure in the Mechanical Behavior of Metals. ASD-TDR-63-234, AFSC, Wright Patterson Air Force Base, Ohio, 243.
Mecking, H., Kocks, U.F., 1981. Kinetics of flow and strain-hardening. Acta Metall. 29, 1865–1875.
Mills, D., Craig, G.B., 1968. The plastic deformation of zirconium–oxygen alloy single crystals in the range 77 to 950 K. Trans. Metal Soc. AIME 242, 1881–1890.
Monnet, G., Devincre, B., Kubin, L.P., 2004. Dislocation study of prismatic slip systems and their interactions in hexagonal close packed metals: application to zirconium. Acta Mater. 52, 4317–4328.
Mordehai, D., Ashkenazy, Y., Kelson, I., 2003. Dynamic properties of screw dislocations in Cu: a molecular dynamics study. Phys. Rev. B 67, 024112-1–024112-9.

Partridge, P.G., 1967. The crystallography and deformation modes of hexagonal close-packed metals. Metall. Rev. 12, 168–194.

Peeters, B., Seefeldt, M., Teodosiu, C., Kalidindi, S.R., Van Houtte, P., Aernoudt, E., 2001. Work-hardening/softening behaviour of BCC polycrystals during changing strain paths: I. An integrated model based on substructure and texture evolution, and its prediction of the stress–strain behaviour of an IF steel during two-stage strain paths. Acta Mater. 49, 1607–1619.

Perlovich, Y., Isaenkova, M., Fesenko, V., Grekhov, M., Yu, S.H., Hwang, S.K., Shin, D.H., 2005. Mater. Sci. Forum, 859–864.

Plunkett, B., Lebensohn, R.A., Cazacu, O., Barlat, F., 2006. Anisotropic yield function of hexagonal materials taking into account texture development and anisotropic hardening. Acta Mater. 54, 4159–4169.

Pontes, J., Walgraef, D., Aifantis, E.C., 2006. On dislocation patterning: multiple slip effects in the rate equation approach. Int. J. Plasticity 22, 1486–1505.

Price, P.B., 1963. Direct observations of glide, climb, and twinning in hexagonal metal crystals. In: Electron Microscopy and Strength of Crystals. John Wiley and Sons, NY, pp. 41–130.

Proust, G., Tomé, C.N., Kaschner, G.C., 2007. Modeling texture, twinning and hardening evolution during deformation of hexagonal materials. Acta Mater. 55, 2137–2148.

Rapperport, E.J., Hartley, C.S., 1960. Deformation modes of zirconium at 77, 575, and 1075 K. Trans. Metall. Soc. AIME 218, 869–876.

Reed-Hill, R.E., Slippy Jr., W.A., Buteau, L.J., 1963. Determination of alpha zirconium {1121} twinning elements using grain boundary rotations. Trans. Metall. Soc. AIME 227, 976–979.

Reed-Hill, R.E., Dahlberg, E.P., Slippy Jr., W.A., 1965. Some anelastic effects in zirconium at room temperature resulting form prestrain at 77 K. Trans. Metall. Soc. AIME 233, 1766–1771.

Reed-Hill, R.E., Iswaran, C.V., Kaufman, M.J., 1995. A power law model for the flow stress and strain rate sensitivity in CP titanium. Scripa Metall. Mater. 33, 157–162.

Rollett, A.D., Kocks, U.F., Stout, M.G., Embury, J.D., Doherthy, R.D., 1987. Modeling of large strain work-hardening. J. Met. 39, A22.

Saada, G., 1963. Dislocation interactions and plastic deformation of crystals. Electron Microscopy and Strength of Crystals. John Wiley and Sons, New York, pp. 651–663.

Saada, G., 1994. Dynamical effects in crystal plasticity. Key Eng. Mat. 97–98, 275–286.

Salem, A.A., Kalidindi, S.R., Semiatin, S.L., 2005. Strain hardening due to deformation twinning in {alpha}-titanium: Constitutive relations and crystal-plasticity modeling. Acta Mater. 53, 3495–3502.

Sarma, G., Zacharia, T., 1999. Integration algorithm for modeling the elasto-viscoplastic response of polycrystalline materials. J. Mech. Phys. Solids 47, 1219–1238.

Seeger, A., Mader, S., Kronmuller, H., 1963. Electron Microscopy and Strength of Crystals. John Wiley and Sons, New York, pp. 665–712.

Serra, A., Pond, R.C., Bacon, D.J., 1991. Computer simulation of the structure and mobility of twinning dislocations in h.c.p. metals. Acta Metall. Mater. 39, 1469–1480.

Song, S.G., Gray III, G.T., 1995a. Structural interpretation of the nucleation and growth of deformation twins in Zr and Ti – I. Application of the coincidence site lattice (CSL) theory to twinning problems in h.c.p. structures. II. TEM study of twin morphology and defect reactions during twinning.. Acta Metall. Mater. 43, 2325–2350.

Song, S.G., Gray III, G.T., 1995b. Influence of temperature and strain rate on slip and twinning behavior of Zr. Metall. Mater. Trans. A 26, 2665–2675.

Soo, P., Higgins, G.T., 1968. The deformation of zirconium–oxygen single crystals. Acta Metall. 16, 177–186.

Stohr, J.F., Poirier, J.P., 1972. Electron microscope study of pyramidal $\{11\bar{2}2\}\langle 11\bar{2}3\rangle$ slip in magnesium. Phil. Mag. 25, 1313–1329.

Stroh, A.N., 1955. Brittle fracture and yielding. Phil. Mag. 46, 968–972.

Swann, P.R., 1963. Dislocation arrangements in face-centered cubic metals and alloys. In: Electron Microscopy and Strength of Crystals. John Wiley and Sons, NY (Chapter 3, pp. 131–181).

Takeuchi, T.Y., 1970. Theory of high-temperature type work-hardening of body-centred cubic metals. J. Phys. Soc. Jpn. 28, 955–964.

Thompson, N., Millard, D.J., 1952. Twin formation in cadmium. Phil. Mag. 43, 422–440.

Tomé, C.N., Kaschner, G.C., 2005. Modeling texture, twinning and hardening evolution during deformation of hexagonal materials. Mater. Sci. Forum 495–497, 1001–1006.

Tomé, C.N., Lebensohn, R.A., 2004. Self consistent homogenization methods for texture and anisotropy. In: Raabe, D., Roters, F., Barlat, F., Chen, L.Q. (Eds.), Continuum Scale Simulation of Engineering Materials:

Fundamentals, Microstructures, Process Applications. Wiley–VCH Verlag GmbH & Co., KGaA, Weinheim, pp. 473–499.
Tomé, C.N., Maudlin, P.J., Lebensohn, R.A., Kaschner, G.C., 2001. Mechanical response of zirconium. Part I: derivation of a polycrystal constitutive law and Finite Element analysis. Acta Mater. 49, 3085–3096.
Tonda, H., Ando, S., 2002. Effect of temperature and shear direction on yield stress by {1122}⟨1123⟩ slip in HCP metals. Metall. Mater. Trans. 33A, 831–836.
Walde, T., Riedel, H., 2003. Interactive texture and finite element simulation for modeling of complex deformation processes for hcp metals. Mater. Sci. Forum 426–432, 3679–3684.
Wang, Z.Q., Beyerlein, I.J., LeSar, R., 2007. Dislocation motion in high-strain-rate deformation. Phil. Mag. 87, 2263–2279.
Westlake, D.G., 1961. Twinning in zirconium. Acta Metall. 9, 327–331.
Whelan, M.J., 1959. Dislocation interactions in face-centred cubic metals, with particular reference to stainless steel. Proc. Roy. Soc. (London) A 249, 114.
Yapici, G.G. et al., in press.
Yoo, M.H., 1969. Interaction of slip dislocations with twins in hcp metals. Trans. Metal Soc. AIME 245, 2051–2060.
Yoo, M.H., Lee, J.K., 1991. Deformation twinning in h.c.p. metals and alloys. Phil. Mag. A63, 987–1000.
Yoo, M.H., Loh, B.T.M., 1970. Structural and elastic properties of zonal twin dislocations in anisotropic crystals. In: Simmons, J.A., De Wit, R., Bullough, R. (Eds.), Fundamental Aspects of Dislocation Theory. Nat. Bur. Stand. (US) Special Publication 317, vol. 1, pp. 479–493.
Yoo, M.H., Wei, C.T., 1966. Slip modes of hexagonal-close-packed metals. Phil. Mag. 14, 573–587.
Yu, S.H., Chun, Y.B., Hwang, S.K., Shin, D.H., 2005. Texture development and Monte-Carlo simulation of microstructure evolution in pure Zr grain-refined by equal channel angular pressing. Phil. Mag. 85, 345–371.